Clean Growth*

Costas Arkolakis
Yale University

Conor Walsh
Columbia University

September 2024

Abstract

We provide a spatial theory of clean growth to assess the global impact of the rise of renewable energy. We model the details of the combined production and transmission network of electricity ("the grid") that determine the supply and losses of energy in space. The local rate of clean energy adoption depends on learning-by-doing, the global electricity and trade network, and regional comparative advantage in renewable resources. We use the model to measure the aggregate and spatial implications of clean growth. We find that the world's power system is likely to be dominated by renewables by 2040 in a range of scenarios, with substantial welfare gains, even in the absence of policy. Incorporating policy, we find that the US Inflation Reduction Act significantly accelerates renewable uptake, and generates substantial economic benefits. In addition, planned grid improvements lower prices substantially in many areas of the US, justifying their cost of construction.

*We are grateful to the National Science Foundation for support under Grant #2117288, as well as for the support of the Planetary Solutions Project at Yale and The Tamer Center for Social Enterprise at Columbia Business School. Felipe del Canto Monge, Kerry Nietzel, and Kevin Yin provided outstanding research assistance. We thank Rodrigo Adao, Steven Berry, Julieta Caunedo, Jonathan Dingel, Pablo Fajgelbaum, Kennenth Gillingham, Esteban Rossi-Hansberg, Abdullah Jallow, and William Nordhaus for useful comments and insights, and David Hemous and Derek Lemoine for excellent discussions.

1 Introduction

The arrival of cheap renewable technologies is reshaping global energy use, power production, and trade. Beginning from virtually zero in the mid 2000's, the share of global electricity produced by new solar and wind technologies has begun to rise rapidly (see top panel of Figure 1). Underpinning this trend, costs for renewables have fallen precipitously (see bottom panel of Figure 1). Wind and solar are now the among the cheapest forms of energy in many parts of the world (Roser (2020)).[1] Furthermore, costs are expected to continue to fall with overall capacity installation, a trend the literature has attributed to technical progress and "learning by doing".[2]

These technological trends provide several opportunities. To begin with, they make decarbonization goals much more achievable than thought even a decade ago. Beyond this, they promise substantially cheaper energy. Governments have recently directed substantial resources to decarbonizing electricity grids and encouraging electrification. But what is the role for policy in shaping these technological trends? What are the gains from clean energy subsidies? And given that the existing electricity grid was not built with renewables in mind, how do spatial frictions affect prices and adoption?

In order to answer these questions, we build a theory of clean growth. We focus on two key concepts: the continued cost declines for renewables, and the core spatial nature of the renewable transition. To do so, we embed the details of the combined production and transmission of electricity ("the grid") in a spatial growth model. We then use newly collected data on the global transmission grid, renewable energy potential, and existing fossil assets to quantify the impact of renewables across regions and sectors.

We start in Section 2 by modeling the details of the electricity production network. Electrical power can be generated from fossil or renewable assets in each region. We use the physical properties of the electrical grid to develop a model of transmission and losses of electricity in space, and analyze the net supply of electricity of each region. The demand for electricity is determined by a multi-sector Armington trade model, as in Armington (1969) and Anderson (1979). Prices of electricity are set for a set of regions by a local utility planer depending on the supply and demand for electricity in each node. We show that in equilibrium, the prices chosen by the utility planner are unique, and the corresponding allocations are efficient.

In Section 3, we incorporate this setup in a model of investment in renewable assets. Clean growth is driven by learning by doing in renewable capital. Local investment in renewable technology

[1] In the Supplementary Material for the paper we show that the decline of the investment costs for renewables has rivaled declines for computers and software. In particular, since the introduction of the first commercial silicon-based photovoltaic panel by Bell laboratories in 1956 for use in the satellite industry (see e.g. Perlin (1999) Chapter 6), photovoltaic costs have been declining at an average rate of about 15% per year.

[2] See, for example, McDonald and Schrattenholzer (2001) ,Van Benthem et al. (2008), Baker et al. (2013), Rubin et al. (2015), Newbery (2018), Roser (2020).

Figure 1: Progress in Clean Energy

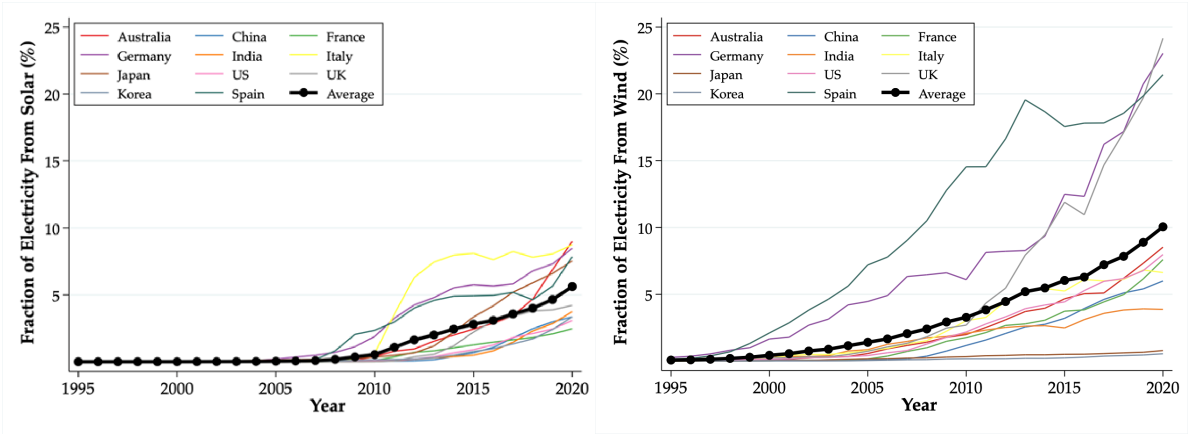

(a) Renewable Energy Adoption

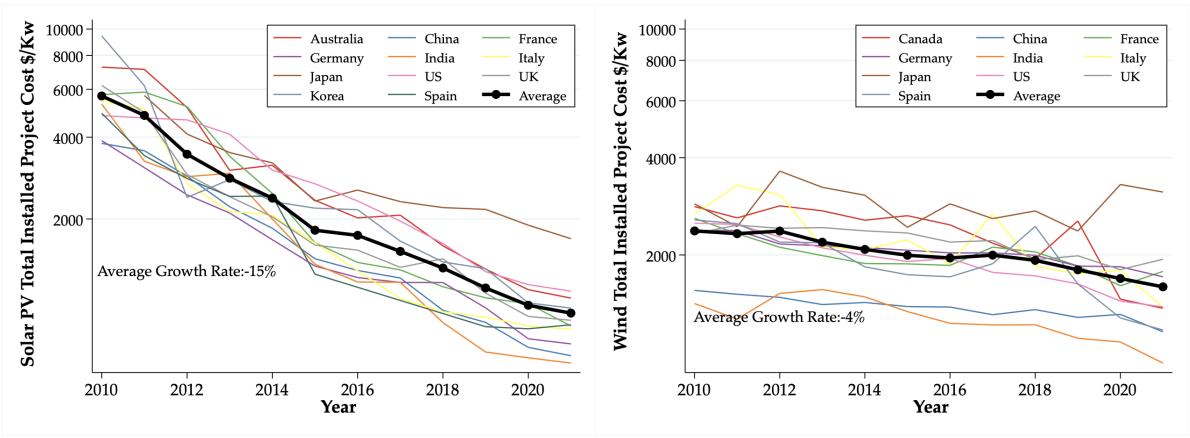

(b) Solar Energy and Onshore Wind Energy Costs

Notes: The top panels plot the share of a country's total electricity usage that comes from solar or wind for a set of major industrial countries. The right panel plots the levelized cost of energy from a new solar or wind energy project across countries in 2019 dollars. Data comes from the International Renewable Energy Agency.

depends on local electricity prices now and in the future. The speed of adoption in a given location is determined by the spatial productivity of the renewable capital, which depends on local renewable potential, local economic conditions, and the structure of the electricity grid. As more renewable capital is installed globally, investment prices fall continually due to global spillovers from learning by doing. This pushes down wholesale power prices on the electricity network, and drives increases in output.

To create a quantitative portrait of the transition to renewable energy, we also incorporate fossil capital investment. In addition, we model the supply of fossil fuels as arising from a dynamic fossil fuel extraction problem. This allows us to measure the income losses faced by fossil-rich countries. Finally, we assume that renewable installation may need to be paired with batteries to deal with intermittency, or face curtailment, as their electricity output is variable over both daily and seasonal horizons.

In Section 4, we complement the theory with several newly constructed datasets, harmonized at the regional level. We use a comprehensive database of the world's power plants to measure current fossil and renewable capital. We incorporate information on renewable potential at a very fine spatial disaggregation for solar and wind technologies. Finally, we construct a new database on global electricity transmission networks and their connections.

In Section 5, we use our quantitative model to trace out the implications of clean growth for welfare across the globe. We find that, in our baseline case with no subsidies, renewables quickly dominate the electric grid, rising to over 70% of world power output by 2040. Their adoption leads to dramatic falls in power prices, which fall on average by over 50% in the same time. The subsequent increase in industrial output raises welfare by an average of 4.6%, though with substantial heterogeneity across the globe. The need for storage slows the transition somewhat, and in a medium storage scenario renewables account for 50% of world power output by 2040. We additionally compare the path of the model to a world in which technical progress in renewables is exogenous under a range of scenarios.

Lastly, we consider the role of policy in shaping the transition. In particular, we model the effects of the Inflation Reduction Act (IRA) passed by the Biden administration in 2022. Among other things, this included a substantial production tax credit for new renewable energy of $26 per mWh. We incorporate this subsidy into the model and solve for the induced change in the energy transition relative to our baseline.

We find that the IRA significantly hastens the adoption of renewable energy in the US, increasing renewable penetration by around 13% by 2030. It also has global spillovers, as the increased investment drives capital prices lower, increasing adoption in other countries around the world. The budgetary cost is substantial, coming in close to the budgeted cost of $160 billion. Much of the subsidy goes to inframarginal investment, which would have been installed in the absence of the

IRA. Nonetheless, even without considering any benefits of carbon pollution reduction, we find that the IRA more than pays for itself.

We finally model the impact of grid expansion. To do so, we collect data on several major proposed grid enhancements, which improve the capacity for power transfer between US regions. We solve for a counterfactual long run steady state with these enhancements, and find that they lower prices substantially in many areas of the US, as well as justifying their cost of construction.

Overall, the picture that emerges from our analysis is of a world undergoing rapid, beneficial change. Under all scenarios we consider, world power production is likely to shift fairly quickly to a grid dominated by renewables, bringing with it cheaper power and greater industrial output. Importantly, this conclusion holds when we conduct our analysis under a fixed transmission grid; we do not find the current grid structure in most countries to be inimical to renewable investment. As we discuss below, the modular nature of renewables and the speed of ongoing cost falls means that significant welfare gains are likely even without additional investment in grid infrastructure. In ongoing work, we consider the role of improving transmission linkages in further hastening clean growth.

Related Literature. A large literature in energy economics has built multi-sector integrated assessment models to evaluate the medium and long-run macroeconomic effects of renewable adaption based on Computable General Equilibrium models (see Baker et al. (2013) for a review).[3] Although we incorporate a comprehensive, multi-sector depiction of the economy, our examination takes place at the regional level, which is crucial due to the regional differences in electricity generation and efficiency of renewable energy. We further contribute to this literature by considering the details of the electricity grid, modeling electricity produced using various alternative sources and transmitting to other locations. [4] Lastly, but importantly, our analysis inherits the welfare-theoretical rigor and the relative tractability of modern quantitative trade and spatial models.[5]

We contribute to the literature analyzing economic growth and the growth of the renewables sector and energy in particular. As pointed out by Stern (2019), "the core mainstream economic

[3]At the same time, energy usage has been recently the topic of work in industrial organization (see, for example, Asker et al., 2019; Hodgson, 2019). Other academic work, such as Golosov et al. (2014); Kortum and Weisbach (2021); Krusell and Smith Jr (2022) consider optimal taxation of fossil fuels and policies taxing CO2 emissions. Alvarez and Rossi-Hansberg (2021) model the implications of climate change for economic allocations across space with the presence of an energy sector (see also Conte et al. (2021)).

[4]Our paper is related to the integrated assessment model of Bohringer and Loschel (2006). They adapt a "bottom-up" approach to model the electricity sector wherein energy source selections are modeled as a mixed complementarity problem within a Computable General Equilibrium framework. We instead model the choice of energy sources as a "merit order dispatch" common to power network in that power is scheduled from different sources in order of increasing marginal cost and used depending on overall energy needs.

[5]See Redding and Rossi-Hansberg, 2017 and Costinot and Rodríguez-Clare, 2014 for in-depth reviews of quantitative spatial and trade models. A feature of our setup is that given electricity prices, determined by the grid, it retains several of the properties of standard spatial models and allows for the use of the standard techniques of solving for the equilibrium and model counterfactuals (see e.g. Allen and Arkolakis (2014)). Likewise, we show how to tractably model investment dynamics in a multi-region, multi-sector setup by exploiting the modularity of renewable investment and assuming free entry into renewable investment (see Walsh (2021) for a similar approach).

growth models disregard energy or other resources". There are, however, some growth models that incorporate energy usage. For example, Tahvonen and Salo (2001) and Fröling (2011) provide a theoretical analysis of the use of renewable energy in a unified growth framework. Acemoglu et al. (2012) model the endogenous adoption and development of clean vs. dirty inputs into production in a directed technical change framework (see also Acemoglu et al. (2014)). Relative to these papers, we model the physical properties of electrical transmission and generation, and stress the spatial dimension of the analysis, given the varying productivity of renewables across space and the need to transfer energy from regions with abundant renewable resources to heavily populated or industrialized ones.

Finally, a significant literature in development has empirically evaluated the effects of electrification on productivity either in developing countries or in the context of historical development (see, for example, Rud, 2012; Moretti, 2013; Allcott et al., 2016; Moneke, 2020; Fiszbein et al., 2020; Colmer et al., 2023). In a regional model, electrification has been modeled as an exogenous increase in productivity as in Kline and Moretti, 2014; Moneke, 2020. Instead, our approach emphasizes the endogenous effects that access to electricity has on output through energy prices, and integrates recent developments in the quantitative spatial and trade literature with models that incorporate supply and demand of energy (Nordhaus et al., 1973; Kypreos and Bahn, 2003; Edenhofer et al., 2013). To these latter contributions we add a model of the electricity grid and renewable or traditional power assets. In addition, we deal with intermittency of renewables by allowing renewable investment be paired with batteries, or face curtailment. Lastly, due to the challenges involved in modeling the energy transition at a global level, we abstract from many interesting features of the microeconomics of energy markets and renewable integration; see Wolak (2021) and Tangeras and Wolak (2021).

2 Setup

We consider an electrical grid with J nodes. Each node could be the location of an electricity generator, a location where other economic activity takes place and consumes power, or both. We use bold notation to denote vectors and bold with a bar to denote matrices. We start with the description of the electrical grid, the production of electricity, the associated electricity losses, and the power planning problem that determines electricity prices in each region. Subsequently, we embed this setup in a standard spatial economy setup.

2.1 The Electrical Grid

Each node has a cost of of generation $M_j(Y_j^{\mathcal{E}})$, where $Y_j^{\mathcal{E}}$ is power produced in node $j \in J$. The maximum output of node j is denoted by Y_j^{max}. Each location has demand for power $D_j(p_j^{\mathcal{E}})$, where

$p_j^{\mathcal{E}}$ is the price of power, dictated by trade, aggregate demand and supply of labor, which will be determined by our spatial equilibrium setup.[6] We denote by $\mathbf{P}$ the vector of dimension $J-1$ and its element P_j to be the net power output of node j, such that

$$P_j = Y_j^{\mathcal{E}} - D_j. \tag{1}$$

We clarify below how the power in J^{th} node (also called the *swing bus)* is determined.

The electrical grid consists of power lines that connect a subset of the power nodes. This grid is represented by a matrix $\bar{\boldsymbol{A}}$ of dimension $K \times (J-1)$, with an entry of 1 in the (k,j) cell and -1 in the (k,i) cell if node j is connected to node i via line k. K is the total number of lines. We consider only bilateral links. Power flows on all lines are represented by the vector $\mathbf{Z}$ with element Z_k. Flows can take on positive or negative values; if Z_k is positive it indicates power flowing from node j through line k to i. Each line also has a maximum amount of power that can flow on it, the *transmission capacity*, which we denote as Z_k^{max}, such that $|Z_k| \leq Z_k^{max}$. Lastly, each line has a resistance R_k and an inductance X_k. Both are determined by physical properties of the line, including the line length and materials: Resistance measures how strongly a line resists electrical current flowing through it, while inductance is relevant for AC power networks and measures how strongly a line resists changes in electrical current.

2.2 Electricity Production

Electricity production in a node depends on the amount of power capital installed in that node. Power capital in a node j is owned by the agents who live in the region j. It comes in two forms: renewable ($\mathcal{R}$) and fossil fuel ($\mathcal{F}$), with amounts $K_j^{\mathcal{R}}$ and $K_j^{\mathcal{F}}$, respectively. Renewable capital produces

$$Y_j^{\mathcal{R}} = \theta_j^{\mathcal{R}} K_j^{\mathcal{R}} \tag{2}$$

units of electricity per period, where θ_j is a local renewable potential. That is, renewable capital produces power with no inputs, and at zero marginal cost. There are two types of renewable capital: solar and wind, $\mathcal{R} = \{\mathcal{S}, \mathcal{W}\}$, that differ only in their local potential $\theta_j^{\mathcal{R}}$. Figure 2 plots a representation of this potential across the globe.[7]

Fossil fuel capital instead requires the use of fossil fuel inputs, the total use of which in j is denoted

[6] We assume that the demand for energy is continuously differentiable and decreasing in p_j, and diverges as $p_j \to 0$ We show that these assumptions hold from the energy demand function resulting from the quantitative trade model of Section 2.5.

[7] We consider hydro and nuclear, with their large fixed costs and lack of recent technological progress, to be part of fossil fuel capital. We are primarily interested in modeling power prices, and not emissions. In reality, solar and wind differ also in their intermittency; solar is intermittent at diurnal frequencies, wind is variable over weekly and seasonal horizons. We address intermittency of these technologies below in Section 2.4.

Figure 2: Global Renewable Potential

(a) Solar Potential

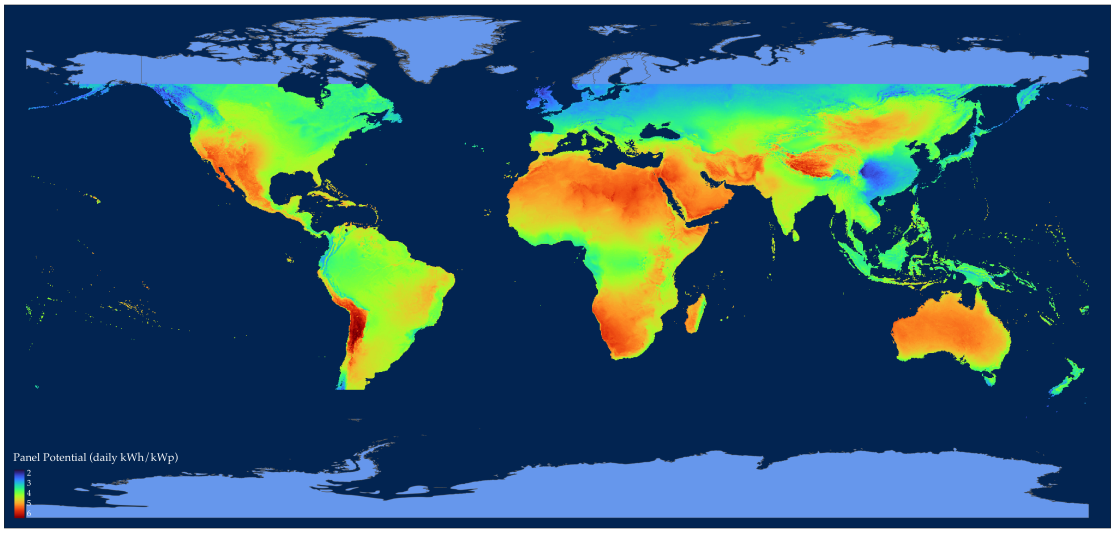

(b) Wind Potential

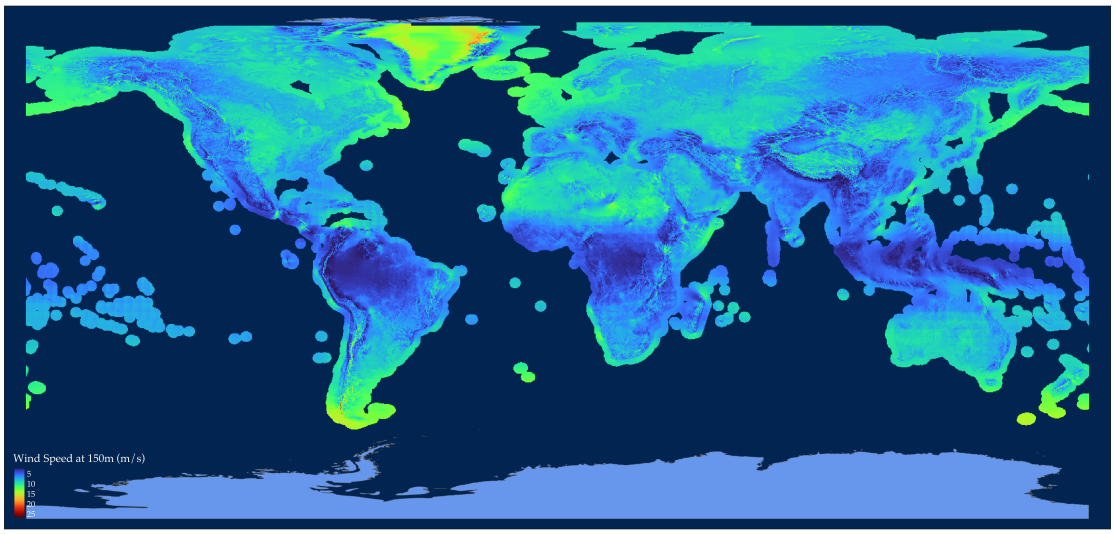

Notes: Panel (a) shows solar panel potential (defined as daily kWh per peak kilowatt rating of the panel) using data from the Global Solar Atlas. Panel (b) shows wind electricity potential (average daily wind speeds) using data from the Global Wind Atlas.

F_j. Producing $Y_j^{\mathcal{F}}$ units of power requires

$$F_j^{\mathcal{E}} = G(K_j^{\mathcal{F}}, Y_j^{\mathcal{F}})$$

units of fossil fuels, where G is continuous and strictly increasing in $Y_j^{\mathcal{F}}$, and for fixed capital $K_j^{\mathcal{F}}$ is convex in $Y_j^{\mathcal{F}}$. We denote the total electricity production as $Y_j^{\mathcal{E}}$ so that

$$Y_j^{\mathcal{E}} = \sum_{\mathcal{R}=\{\mathcal{S},\mathcal{W}\}} Y_j^{\mathcal{R}} + Y_j^{\mathcal{F}}. \tag{3}$$

Fossil fuels are traded globally for a price $p^{\mathcal{F}}$ in units of a final numeraire good (specified below), and can be bought anywhere for the same price. The total cost of producing power $Y_j^{\mathcal{E}}$ is

$$M_j(Y_j^{\mathcal{E}}) = \begin{cases} p^{\mathcal{F}} G_j(K_j^{\mathcal{F}}, Y_j^{\mathcal{E}} - \sum_{\mathcal{R}=\{\mathcal{S},\mathcal{W}\}} \theta_j^{\mathcal{R}} K_j^{\mathcal{R}}) & \text{if } Y_j^{\mathcal{E}} > \sum_{\mathcal{R}} \theta_j^{\mathcal{R}} K_j^{\mathcal{R}} \\ 0 & \text{if } Y_j^{\mathcal{E}} \leq \sum_{\mathcal{R}} \theta_j^{\mathcal{R}} K_j^{\mathcal{R}} \end{cases}$$

This formulation reflects the process of "merit order dispatch" common to power networks: the lowest marginal cost power stations are dispatched to supply the grid (the operation of which is described below), then power is scheduled in order of increasing marginal cost. The availability of renewables has significant effects on merit order dispatch prices, as they typically have much lower marginal costs than traditional forms of energy (see Woo et al. (2016); Clo et al. (2015) for California and Italy, respectively).

Lastly, there is a maximum fossil fuel input F_j^{max} , such that maximum power production in a node is

$$Y_j^{\mathcal{E}} \leq Y_j^{max}.$$

This captures the notion that power stations have a rated maximum power capacity. Generation capacities are readily available across the world, and we will use them for our calibration in Section 4.

2.3 Electricity Losses

The distribution of electric power across the lines in the grid incurs losses. However, flows cannot be allocated to a line. They are determined from Kirchhoff's laws and the amount of generation and consumption in each node (Decker, 2021) and must at all times satisfy the energy balance constraint

$$\sum_j D_j + \lambda = \sum_j Y_j^{\mathcal{E}}, \tag{4}$$

so that total energy used, plus total systems losses λ, is equal to that produced across all power assets.

Based on these properties of the grid and the power flow, we show in Appendix A4 that we can approximate the loss in each line in the grid as $\lambda_k = R_k Z_k^2$ (see also Bohn et al. (1984); Cretì and Fontini (2019)). The total transmission loss function is a function of all of these flows, denoted $\lambda(\mathbf{Z})$ and is (approximately) given by

$$\lambda(\mathbf{Z}) = \sum_k R_k Z_k^2. \tag{5}$$

Our next aim is to derive the total loss on the network as a function of net power in each node j and the transmission network features. In the Appendix, we show that the relationship between power in each line and the power nodes can be written as

$$\mathbf{Z} = \bar{\mathbf{\Omega}}\bar{\boldsymbol{A}}(\bar{\boldsymbol{A}}'\bar{\mathbf{\Omega}}\bar{\boldsymbol{A}})^{-1}\boldsymbol{P}, \tag{6}$$

where $\bar{\mathbf{\Omega}}$ is a $K \times K$ diagonal matrix of "line admittances" such that $\Omega_k = (R_k^2 + X_k^2)^{-\frac{1}{2}}$ (i.e. its elements are inversely related to resistance R_k and inductance X_k). We assume for the remainder of the paper that inductance and resistance are proportional.

Now since line losses are given by (5), we can express losses in terms of the characteristics of the network and the power generated by each asset according to the following lemma:

Lemma 1. *Power losses in the system can be expressed in a quadratic form:*

$$\lambda = \boldsymbol{P}'\bar{\boldsymbol{B}}\boldsymbol{P} \tag{7}$$

where

$$\bar{\boldsymbol{B}} = (\bar{\boldsymbol{A}}'\bar{\boldsymbol{R}}^{-1}\bar{\boldsymbol{A}})^{-1} \tag{8}$$

is a positive semi-definite $(J-1) \times (J-1)$ matrix of fundamentals and $\bar{\boldsymbol{R}}$ is a $K \times K$ diagonal matrix of line resistances.

This representation of transmission losses — its elegance notwithstanding — is useful for two purposes. First, it allows us to express the relation between losses in the network and power generation across nodes in terms of the measurable features of the network summarized in the matrix $\bar{\boldsymbol{B}}$, using information from the power network linkages and their associated resistances. Given the net output power of each node, this information is a sufficient statistic for the losses in the system. Second, the fact that $\bar{\boldsymbol{B}}$ is positive semi-definite is important in allowing us to characterize the power network planning problem.

Figure 3: The United States Transmission Grid

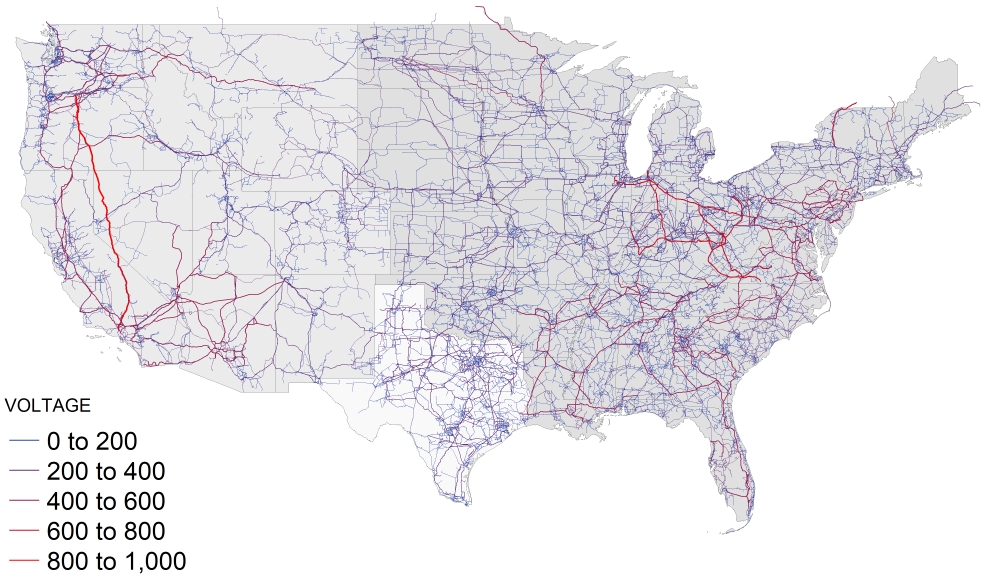

Notes: This Figure shows the high voltage transmission network of the United States as well as the interconnections between the networks using data from the U.S. Energy Information Administration. While there are a few small interconnections between the three networks, they are effectively independent.

2.4 The Power Network Planning Problem

We assume the presence of a centralized power network administrator over a collection of connected nodes $\mathcal{T}$. This administrator aims to maximize economy wide output net of generation costs by setting local electricity prices, while balancing supply and demand of electricity. For example, in the continental United States the power grid is made up of three main interconnected transmission networks: the Eastern Interconnection encompasses the area east of the Rocky Mountains and a portion of the Texas panhandle, the Western Interconnection encompasses the area to the west of the Rocky Mountains, and the Electric Reliability Council of Texas (ERCOT) which covers most of Texas. While there are minimal connections between these three transmission networks, the power capacity of these connections is very small, and we treat these networks as independent. Thus, the power grid mechanics described above will hold for each of these networks separately.[8] In Figure 3 we depict the entire continental United States network. The areas covered by the three power transmission networks are shaded with a different gray.

[8]Within both the Western and Eastern Interconnections, there are additional entities called Regional Transmission Organisations (RTOs) or Independent System Operators (ISOs), that administer wholesale power markets and operate the electricity grid within their geogrpahic area. Examples include PJM for Pennsylvania, New Jersey and other Mid-Atlantic Areas, and the New England ISO. In reality, these RTOs are the relevant administrators corresponding to our problem, but for simplicity we aggregate to the Interconnection level for the US. In doing so, we abstract from trade between RTOs within Interconnections, and plan to pursue this in future work.

We assume that the network administrators have an objective for each location $Q_j(p_j^{\mathcal{E}})$, which is strictly decreasing in the price of that location, $p_j^{\mathcal{E}}$. We put further structure on this objective below, but keep it general here for exposition. As above, M_j is the cost of generating energy output $Y_j^{\mathcal{E}}$ in node j, in units of the final good. The problem of the administrator is to choose prices $\{p_j^{\mathcal{E}}\}$ in the nodes that it administers in order to solve

$$\max_{\{p_j^{\mathcal{E}}\}} \sum_j Q_j(p_j^{\mathcal{E}}) - \sum_j M_j(Y_j^{\mathcal{E}}(p_j^{\mathcal{E}})) \tag{9}$$

subject to the net power production in each power node equation (1), the energy balance constraint in equation (4), equation (7) that determines the losses in the network, the power in each link equation (6), and the network constraint for each link, $Z_k \leq \bar{Z}_k^{max}$.

We assume that any profits or losses of the electricity network are rebated uniformly to the consumers that correspond to the administrative boundaries of each transmission network. While it is simple to show that the price of electricity is always weakly higher in nodes that are net users of power, it does not follow that the electricity network always makes a positive profit, since they must absorb transmission losses. The associated profits or losses from the operation of the electricity network in a region j belonging to the transmission network $\mathcal{T}$ are denoted by

$$\Pi_j^{\mathcal{T}} = \sum_{i \in \mathcal{T}} p_i^{\mathcal{E}} \left(D_i - Y_i^{\mathcal{E}} \right) \frac{L_j}{\sum_{i \in \mathcal{T}} L_i},$$

where L_j is population of region j, and D_i is total power demand in region i.

Intermittency. So far we have ignored the intermittency of electricity production of renewable capital, which is a central issue in the uptake of this technology. The output of fossil fuel capital is largely predictable and can be scheduled and controlled in advance (severe weather events such as the Texas blackout of 2021 notwithstanding). This is not as true for solar and wind energy sources.

There are two dimensions to this intermittency. First, there is a strong seasonal component to electricity produced from renewable electricity (Mulder, 2014). On the one hand, outside of the equator, solar capital produces significantly less electricity in the winter. On the other hand, wind speeds tend to be higher in the winter in many places on the planet. Within the model, this can be handled in a natural way, by defining the period t to occur at the sub-year level, and allowing the renewable potential $\theta_j^{\mathcal{R}}$ to depend on calendar time t. We plan to pursue this extension in future work.

Second, renewable electricity production has marked variation on a daily time scale, fluctuating substantially from day to day for both wind and solar capital (depending on wind speeds, and cloud cover and night, respectively). Due to the complexity of doing so at a world scale, we avoid modeling the stochastic scheduling problem of each utility directly, which involves setting variable

wholesale prices across different periods of the day in response to both predicted and observed weather patterns.

The seasonal and daily variation in renewable production brings about two important economic considerations. First, depending on renewable capacity build and geophysical constraints (see Shaner et al. (2018)), there is a significant possibility of excess generation that needs to be taken into account. This can equivalently be thought of as overbuilding renewable capital to meet times of peak demand, and then wasting electricity output at times of low demand and it can an economical outcome. We incorporate estimates of curtailment modeled as efficiency loses in electricity generation of renewables using the recent measurements of Tong et al. (2021) based on The geophysical constraints such as the seasonal and daily variations mentioned above, but also additional ones such as the structure of the grid infrastructure, time zone variation and other.

Second, this variation in output provides substantial opportunities for battery arbitrage as battery prices continue to fall (Nykvist and Nilsson, 2015). While stand-alone merchant batteries are beginning to be observed, direct pairing with renewable generation assets is also likely (Gorman et al., 2022). We address this consideration by modeling simple scenarios for the the adoption of battery storage in a range of capacities, taking into account engineering estimates for the cost of batteries and the projection for future cost declines, avoiding modeling the dynamic stochastic problem of storage directly.

Limitations. Our model of the electrical grid is necessarily simplified. We abstract from several important features, including control of reactive power, and the inertial and grid-forming services of various different power generation technologies (see e.g. Mehigan et al. (2020)). We also ignore constraints on voltage control, and reliability metrics. Doing so in a tractable manner is an important future challenge for both policymakers and economists studying the renewable transition.

2.5 A Spatial Economy with Power

We embed the energy sector in a dynamic multi-region, multi-sector spatial economy. The consumer has Cobb-Douglas preferences over goods from different sectors s,

$$C_j = \prod_s C_{js}^{\beta_{js}},$$

where β_{js} is the consumption share of region j in sector s.

For each sector s each region j produces a differentiated good as in Armington (1969) and these goods are aggregated through a standard constant elasticity aggregator with an elasticity across varieties σ_s. Labor is fully mobile across sectors within the regions, and we denote the wage rate in region j by w_j.

The production of the differentiated good for the amount the regional good j is given by

$$q_{js} = z_{js} \left(e_{js}^1\right)^{v_{js}^{\mathcal{E}}} \left(\kappa_{js} \left(e_{js}^2\right)^{\frac{\psi-1}{\psi}} + f_{js}^{\frac{\psi-1}{\psi}}\right)^{\frac{\psi}{\psi-1} v_{js}^{\mathcal{F}}} k_{js}^{v_{js}^K} L_{js}^{v_{js}^L}, \tag{10}$$

where for each region j, sector s, and time t, z_{js} is a regional productivity shifter, L_{js} is the amount of labor used, e_{js}^1 is the direct amount of electricity used in production, and e_{js}^2 is secondary use of electricity that is directly substitutable with the additional use of fossil fuels f_{js}. The production capital is denoted by k_{js} and the total production capital in a region is denoted by $K_j^P \equiv \sum_s k_{js}$. We assume that $v_{is}^{\mathcal{E}} + v_{is}^{\mathcal{F}} + v_{is}^K + v_{is}^L = 1$ for all i and s. Lastly, there is an iceberg trade cost τ_{ijs} for shipping a unit of the good from i to j in sector s.

Electricity plays two roles in the production function. e^1 is a direct use for purposes that cannot be typically substituted for fossil fuels, such as lighting, computation or machine power. e^2 is a potential input where employment of fossil fuels is feasible, such as heating or transportation, but electricity usage is also possible. The parameter ψ denotes the elasticity of substitution across electricity and fossil fuels for this input. κ_{js} is a fixed level shifter in the productivity of electricity for indirect use.

Denote total usage of fossil fuels used in production in region j as $F_j^I = \sum_s f_{js}$. Each region also has a certain supply of fossil fuels, which it sells freely for the world market price $p^{\mathcal{F}}$ and yield profits $\Pi_{j,t}^{\mathcal{F}}$. We determine the optimal extraction problem and the associated profits below.

We denote the price of a good s from region i sold in j as p_{ijs}. Total sales for each sector in each region, are given by

$$X_{is} = \sum_j p_{ijs} Y_{ijs} = \sum_j \frac{p_{ijs}^{1-\sigma_s}}{\left(P_{js}^{\mathcal{C}}\right)^{1-\sigma_s}} \beta_{j,s} E_j, \tag{11}$$

where $P_{js}^{\mathcal{C}} = \left(\sum_{i'} p_{i'js}^{1-\sigma_s}\right)^{1/(1-\sigma_s)}$ is the CES price index, and expenditure E_j is given by

$$E_j = \underbrace{w_j L_j}_{\text{labor income}} + \underbrace{r_j^{\mathcal{K}} K_j^P}_{\text{capital income}} + \underbrace{p_j^{\mathcal{E}} Y_j^{\mathcal{E}} - p^{\mathcal{F}} F_j^{\mathcal{E}} + \Pi_j^{\mathcal{T}}}_{\text{net power revenue}} + \underbrace{\Pi_j^{\mathcal{F}}}_{\text{fossil income}}. \tag{12}$$

We now define a period equilibrium, leaving the dynamic determination of capital stocks and fossil fuel supplies (as well as time notation) for the following section.

Definition 1. *Given capital endowments $\{K_j^{\mathcal{P}}, K_j^{\mathcal{F}}, K_j^{\mathcal{R}}\}$, labor endowments, $\{L_j\}$ and a supply of fossil fuels $\{F_j^S\}$, a period equilibrium is a vector of prices for the sectoral intermediates $\{p_{ijs}\}$, a vector of wages $\{w_j\}$ and returns on capital $\{r_j^K\}$, a global fossil price, $p^{\mathcal{F}}$, prices of electricity $\{p_j^{\mathcal{E}}\}$, and an allocation $\{k_{js}, l_{js}, f_{js}, Y_j^{\mathcal{E}}, e_{js}^1, e_{js}^2\}$ such that:*

1. *The markets for sectoral intermediates clears (equation (11))*
2. *The labor and production capital markets clear in each location*
3. *The world fossil fuel market clears*
4. *The electricity utility in each region $\mathcal{T}$ solves (9) subject to (1), (4), (6), (7), and for each link, $Z_k \leq \bar{Z}_k^{max}$.*

We now assume that the utility has an objective function that maximizes total regional Gross Domestic Product (GDP), taking output prices as given. That is, they set prices across the network in a way that maximizes the GDP of the regions they serve, given the constraints on the network.

Proposition 1. *If the utility planner's objective function is*

$$Q_j = \sum_s p_{js} q_{js}(D_{js}(p_j^{\mathcal{E}})), \tag{13}$$

where $D_{js} = e_{js}^1 + e_{js}^2$, then the problem has a unique solution, and can be implemented by setting spatial prices in each node i according to

$$p_j^{\mathcal{E}} = \mu + \mu \frac{\partial \lambda}{\partial D_j} + \sum_k \eta_k \frac{\partial Z_k}{\partial D_j}, \tag{14}$$

where η_k is the shadow value of extra capacity on a constrained line k, and μ is the shadow value of total generation capacity.

The price of electricity in any node consists of three components. First, μ, is the marginal system generating cost, determined by the cost of the last unit of electricity generation used by the grid, and is the same everywhere. Second, the utility planner adjusts prices by the marginal impact on the losses of demanding more (net) power in a location j. This term may be positive or negative; it may be that increasing power demand in a node j decreases flows on congested lines elsewhere, and brings losses down at the network level. The last term is determined by the overall line capacity constraints. When lines are at capacity in the system, increasing power withdrawal at node j may not be possible without burning out a fully loaded transmission line. As such, demand must be discouraged by raising the price in j so that the line remains fully loaded.

Pricing formulas such as (14) are known in the electricity industry as Locational Marginal Pricing (LMP), since they differ across space in ways that reflect the marginal impact of additional demand or generation, as well as transmission usage costs, on total system performance. It is worth noting that while many utilities use some version of (14), others do not.[9]

[9] In the US, around 80% of US generation assets operate under LMP. In Europe, nodes are organized into collections called zones, with the same price charged within the zone. This can be thought of as another form of LMP with additional constraints on prices. See Decker (2021) and Tangeras and Wolak (2021) for an in depth discussion of LMP.

Assuming that all locations in the world participate in markets that are structured in this way is no doubt a serious simplification of reality. However, it has two advantages that make it worthwhile. First, many geographies that do not currently implement full LMP are considering and studying its adoption, given the obvious efficiency advantages over uniform wholesale pricing in a world of decentralized, renewable generation (Australian Energy Market Commission, 2020; European Network of Transmission System Operators for Electricity, 2022). Second, fully specifying how each different country's electricity market operates would render a global analysis infeasible.

In addition, if the planner's objective function is to maximize regional GDP, we have the following proposition.

Proposition 2. *If the grid planner's objective function is given by (13), then the period equilibrium exists, is unique and is efficient.*

The proof shows an equivalence between the period equilibrium and the solution to a global planner's problem under a certain set of Pareto weights. It also includes a derivation and elaboration of the equilibrium conditions in Definition 1. Crucial for this result is that the utility only considers the impact of pricing decisions on regional production, but not regional prices. That is, they take regional output prices as given.

3 Renewables Investment, Fossil Fuel Extraction, and Clean Growth

To analyze the growth of renewables, we now introduce investment in electricity generation capital. We explicitly introduce time, which is discrete and indexed by t, and characterize consumer and firm intertemporal choices.

Capital. The consumer can invest in renewable capital $K^{\mathcal{R}}_{j,t}$ within their location. The law of motion for renewable capital is

$$K^{\mathcal{R}}_{j,t+1} = (1-\delta)K^{\mathcal{R}}_{j,t} + Q^{\mathcal{R}}_{j,t}, \tag{15}$$

where $Q^{\mathcal{R}}_{j,t}$ is the total installation of new renewable capital in j at time t. We suppose that renewable capital can be produced by transforming $I^{\mathcal{R}}_{j,t}$ units of the final good according to

$$Q^{\mathcal{R}}_{j,t} = \Omega_j \left(\sum_{j'} \sum_{i=1}^{\infty} (\mu)^i Q^{\mathcal{R}}_{j',t-i} \right)^{\gamma_{\mathcal{R}}} I^{\mathcal{R}}_{j,t}, \tag{16}$$

where $I^{\mathcal{R}}_{j,t}$ is total investment of the final good in technology $\mathcal{R} = \{\mathcal{S}, \mathcal{W}\}$, and $\Omega^{\mathcal{R}}_j$ is a region specific cost shifter. There is a spillover into local renewable capital production from global production in all previous periods, by which it becomes cheaper to produce a unit of renewable capital if more has been installed worldwide. $\mu < 1$ is a parameter that discounts learning from the

past due to production experience depreciation (Benkard, 2000). The parameter $\gamma_{\mathcal{R}}$ is termed the *learning rate.* This is a "learning-by-doing" formulation with frictionless spillovers across regional borders. While no doubt an approximation, it is helpful to consider the knowledge spillovers as being mostly global and largely exogenous to local decisions. While installation costs across countries show some differences in levels, they have tended to trend downwards at similar rates (see Figure 1).

We assume that the final good can also be converted into two additional types of capital; fossil fuel capital $K^{\mathcal{F}}_{j,t}$ and production capital $K^{\mathcal{P}}_{j,t}$. Both evolve as in (15), but without external learning economies. For fossil fuel capital, this stylized assumption appears well supported in the data: installation costs of fossil fuel capital such as coal and gas appear to have stayed stable or even increased in real terms in recent decades, as pointed out in Lazard (2019).

Money and bonds. There are two additional assets in the world. First, there is a fixed supply of money, which does not depreciate and gives a utility flow to the consumer. Money holdings are denoted $M_{j,t}$. Money is able to be costlessly transferred across the world. It serves as the numeraire good.

Second, the consumer is able to save or borrow via one-period, riskless bonds, denoted by $a_{j,t}$, which promise payment of $R_t \geq 1$ units of money in the following period. Bonds are in zero-net supply worldwide. Since money is freely transferable, the return on these bonds is common across regions. We assume that bonds are in zero net supply worldwide, and bond markets clear in each period, such that

$$\sum_j a_{j,t} = 0. \tag{17}$$

The introduction of frictionlessly tradable bonds and money is a useful addition to the model, since it allows the formation of a single world interest rate that functions to price capital investment decisions in all locations. It recovers the idea that returns on capital should be roughly equal across space, which can break down in spatial growth models that feature immobile, local capitalists (see, for example, Kleinman et al. (2023)).

Fossil Fuel Extraction. An important aspect of the transition into renewables is the corresponding (negative) income effects induced by the transition out of fossil fuels. Countries rich in fossil deposits, such as oil, natural gas, and coal may lose a stream of income associated with extracting those natural resources or licensing that extraction.

Our analysis of the income effects of fossil fuel ownership follows a long tradition in the exhaustible resources literature, beginning with the influential work of Hotelling (1931). We assume that each country c, is a collection of regions, is endowed with a total supply of fossil fuels ordered by extraction costs. The marginal cost of extraction is $\chi(S_{c,t})>0$, where $S_{\mathcal{C},t}$ is the total value of resources extracted up to period t by country c. We also assume that the resources are extracted

off-shore, and that the cost is denominated in terms of units of the final good. Finally, reflecting on evidence such as in Clark and Jacks (2007), we assume that constant technological progress in extraction takes place every year at a rate $g^{\mathcal{F}}$. The extraction problem for fossil fuels at the country level is

$$\Pi^{\mathcal{F}}_{c,t} = \max_{S_{c,t}} \sum_t R^{-1}_{0\to t} \left(p^{\mathcal{F}}_t \left(S_{c,t} - S_{c,t-1} \right) - \left(1 + g^{\mathcal{F}} \right)^{-t} P^{\mathcal{C}}_{c,t} \int_{S_{c,t-1}}^{S_{c,t}} \chi(q')\, dq' \right), \tag{18}$$

where $R_{0\to t} \equiv \prod_{s=0}^{t} R_s$.

Each region j owns a fraction of the country c's fossil fuel endowment that is proportional to their population, such that $\Pi^{\mathcal{F}}_{j,t} = \Pi^{\mathcal{F}}_{c,t} \times L_j / L_c$. Given the presence of a common world interest rate, all regions within a country agree on the optimal rate of extraction.

Household Intertemporal Choice. The intertemporal preferences of the household are

$$U_j = \max_{\{C_{j,t}, M_{j,t}, I^k_{j,t+1}, a_{j,t+1}\}} \sum_{t=0}^{\infty} \beta^t (\log(C_{j,t}) + \epsilon log(M_{j,t})),$$

subject to

$$P^{\mathcal{C}}_{j,t} C_{j,t} + \sum_{k \in \{F, \mathcal{K}, \mathcal{S}, \mathcal{W}\}} P^k_{j,t} I^k_{j,t+1} + a_{j,t+1} = E_{j,t} + R_t a_{j,t} + (M_{j,t} - M_{j,t+1}), \tag{19}$$

where $a_{j,t}$ is the saving in location r in a global, risk-free bond, $P^{\mathcal{A}}_t$ is the price of the savings bond to yield one unit next period (normalized in terms of the price of the world numeraire), and $I^k_{j,t+1}$ is the amount invested in different types of capital. Capital is sunk once installed and cannot be sold, such that $I^k_{j,t+1} \geq 0$. The first order conditions of the household with respect to consumption and savings imply a standard Euler equation for consumption,

$$\frac{C_{j,t+1}}{C_{j,t}} = \beta R_t \frac{P^{\mathcal{C}}_{j,t}}{P^{\mathcal{C}}_{j,t+1}}. \tag{20}$$

Renewable Capital Investment. We assume that each household decides how much to invest total in solar $\mathcal{S}$ and wind $\mathcal{W}$ together. For a given spend in units of money they invest in renewables, they draw a pair of idiosyncratic shocks $\{\eta^{\mathcal{S}}_j, \eta^{\mathcal{W}}_j\}$, one for solar and one for wind, reflecting variability in local project opportunities. Once they have drawn the shocks, they choose whether to invest in a solar or wind project in that location. Owing to the fact that the marginal cost of renewables is very close to zero (see e.g. Baker et al. (2013)) and the investment is modular, the value of a unit of renewable capital of type $\mathcal{R}$, once installed is given by

$$V^{\mathcal{R}}_{j,t}(\eta^{\mathcal{R}}_j) = p^{\mathcal{E}}_{j,t+1} \theta^{\mathcal{R}}_j \eta^{\mathcal{R}}_j + \frac{1-\delta}{R_t} V^{\mathcal{R}}_{j,t+1}(\eta^{\mathcal{R}}_j).$$

Then define the return to investing one dollar in renewable technologies today as

$$V_{j,t}^{\mathcal{R}} = \mathbb{E}[\max\{\frac{V_{j,t}^{\mathcal{S}}(\eta_j^{\mathcal{S}})}{P_{j,t}^{\mathcal{S}}}, \frac{V_{j,t}^{\mathcal{W}}(\eta_j^{\mathcal{W}})}{P_{j,t}^{\mathcal{W}}}\}].$$

We assume that $\eta_j^{\mathcal{S}}$ are distributed Frechet with shape parameter ϱ and a unit scale parameter. Due to the linearity of the value function, the fraction of investment in renewables that flows to solar, denoted $\Theta_{j,t}^{\mathcal{S}}$ each period will be

$$\Theta_{j,t}^{\mathcal{S}} = Prob(\frac{\theta_j^{\mathcal{S}}\eta_j^{\mathcal{S}}}{P_{j,t}^{\mathcal{S}}} \geq \frac{\theta_j^{\mathcal{W}}\eta_j^{\mathcal{W}}}{P_{j,t}^{\mathcal{W}}}) = \frac{\left(\theta_j^{\mathcal{S}}/P_{j,t}^{\mathcal{S}}\right)^{\varrho}}{\left(\theta_j^{\mathcal{S}}/P_{j,t}^{\mathcal{S}}\right)^{\varrho} + \left(\theta_j^{\mathcal{W}}/P_{j,t}^{\mathcal{W}}\right)^{\varrho}}.$$

The expected price of renewable capital is

$$\bar{P}_{j,t} = \Theta_{j,t}^{\mathcal{S}} P_{j,t}^{\mathcal{S}} + (1 - \Theta_{j,t}^{\mathcal{S}}) P_{j,t}^{\mathcal{W}}.$$

where given the linear production function in equation (16), the price of renewable capital of type $\mathcal{R} = \{\mathcal{S}, \mathcal{W}\}$ in region j time t is

$$P_{j,t}^{\mathcal{R}} = \left(\sum_{j'}\sum_{i=1}^{\infty}(\mu)^i Q_{j',t-i}^{\mathcal{R}}\right)^{-\gamma_R} P_{j,t}^{\mathcal{C}}. \tag{21}$$

Free entry into renewable capital implies

$$\bar{P}_{j,t} \geq R_t^{-1}\left(p_{j,t+1}^{\mathcal{E}}\bar{\theta}_{j,t} + (1-\delta)\bar{P}_{j,t+1}\right), \tag{22}$$

where $\bar{\theta}_{j,t} \equiv \Theta_{j,t}^{\mathcal{S}}\theta_j^{\mathcal{S}} + \Theta_{j,t}^{\mathcal{W}}\theta_j^{\mathcal{W}}$, and where this holds with equality if investment is positive in t.

Given capital prices, the price of electricity, $p_{j,t}^{\mathcal{E}}$, is pinned down by this law of motion whenever investment is positive. This in turn determines electricity production $Y_j^{\mathcal{E}}$, and consumption, D_j.

Definition 2. *An equilibrium is a vector of prices for the sectoral intermediates $\{p_{ijs,t}\}$, vector of wages $\{w_{j,t}\}$, a bond price $\{P_t^{\mathcal{A}}\}$, prices of fossil fuels $\{p_t^{\mathcal{F}}\}$, prices of electricity $\{p_{j,t}^{\mathcal{E}}\}$, prices of the renewable capital $\{P_{j,t}^{\mathcal{R}}\}$, allocations of consumption $\{C_{j,t}\}$, renewable capital stock $\{K_{j,t}^{\mathcal{R}}\}$, fossil fuel capital stock $\{K_{j,t}^{\mathcal{F}}\}_t$, production capital stock $\{K_{j,t}^{\mathcal{P}}\}_t$, and country fossil fuel extraction $\{S_{c,t}\}$, such that for each location j and time period t:*

i) within each t, a period equilibrium holds as defined in Definition 1, ii) the bond market clears (equation (17)), iii) the price of each type renewable capital $\{P_{j,t}^{\mathcal{R}}\}$ evolves according to (21), iv) intertemporal consumption choices $\{C_{j,t}\}$ satisfy (20), v) investment in renewables and the associated capital stock $\{K_{j,t}^{\mathcal{R}}\}$ satisfy the free entry condition (equation (22)) if $I_{j,t+1}^{\mathcal{R}} > 0$, with analogous conditions for production capital $\{K_{j,t}^{\mathcal{P}}\}$ and fossil capital $\{K_{j,t}^{\mathcal{F}}\}$, vi) The extraction of fossil fuels $\{S_{c,t}\}$ solves (18) for each country.

A steady state equilibrium is an equilibrium in which all variables are constant. In the steady state, all fossil fuels have been extracted, and electricity is entirely renewable. The existence of a long-run steady state is ensured by the forgetting parameter μ. Without it, perpetual price falls occur.

Importantly, because of the CES specification in our production function (equation (10)), there is always non-zero demand for fossil fuels at a finite price. The reason this occurs is the finite elasticity of substitution at the industry level ψ. The extent of the timeline of the depletion of fossil reserves ultimately depends on the parameter κ_{js} and in our calibrations the depletion of fossil reserves does not happen for hundreds of years.[10] However, even with decarbonization occurring rapidly in the power sector, all fossil fuels are eventually burned in industry. We assume that once all fossil fuels are extracted, the price of fossil fuels is infinite.

4 Quantitative Analysis

We consider a set of sub-national geographies that roughly correspond to local labor market areas for our quantitative analysis. Our regions are commuting areas in the US, and in most European countries NUTS-3 regions. For other countries we attempt the most granular level of aggregation possible, depending on the available data.

We harmonize datasets from different sources so that they correspond to those geographical boundaries. The harmonization procedure constitutes of bringing together datasets from three disparate sets of sources: data from the electricity grid and power assets, remote sensing data for renewable efficiency, data for output and employment, and regional trade data. We describe the data sources below, and provide data construction details in Appendix A2. Further details are provided in the Online Supplementary Material.

4.1 Global Power Grid, Electricity Generation, and Fossil Extraction

We first construct a unified dataset on the global electricity grid. We source data on the length and voltage of high-voltage transmission lines from OpenStreetMap. A full description of our methods for processing the raw data is contained in Appendix A2. Data on global power generation assets comes from the World Resources Institute Database. It contains information on the size of the power plant, the location, the date constructed and the type of fuel and detailed location information. A summary of this data is provided in Appendix A2.

We then construct a simplified representation of the electricity dataset. First, we aggregate transmission capacity between each region. We sum the total capacity of all lines which begin in one region

[10] As Covert et al. (2016) point out, the reserve to consumption ratio of oil, gas, and coal has remained roughly constant over the decades. This provides some evidence that fossil fuels are not going to deplete for many decades to come.

Figure 4: US Electricity Grid and Power Generation Assets

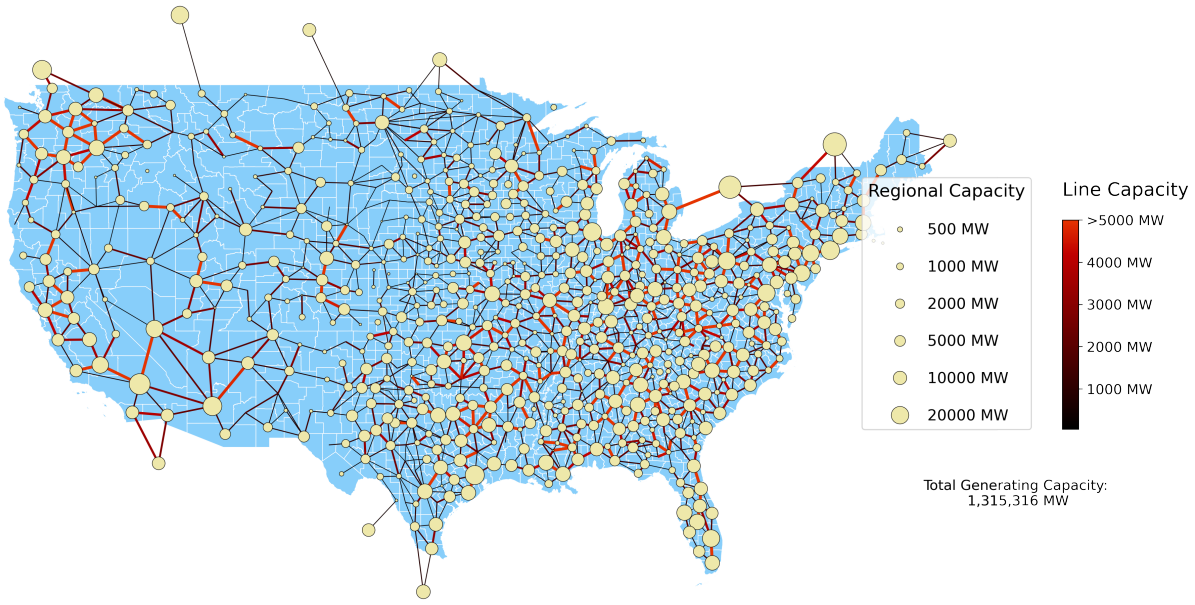

Notes: This figure shows our representation of the electrical grid between regions of the United States using data from OpenStreetMap (transmission lines) and the World Resources Institute Database (power capital). Circle size is proportional to region generating capacity in MW. Line thickness is proportional to transmission capacity between regions. Generating capacities are total nameplate capacity of fossil and clean resources, without adjusting for capacity factors.

and end in another, and compute the distance of transmission as stretching from region centroid to region centroid. Lines which begin and end in the same region are dropped. We then add the total fossil-fuel capacity and renewable capacity (by type) separately, and consider all generation to be done at the region centroid. [11] We code hydro-electricity plants, coal, gas and nuclear as fossil-fuels $\mathcal{F}$, and consider renewables to be solar and wind. The result for North America is presented in Figure 4, and other major regions are presented in the Appendix.[12]

As specified above, we assume renewable generation capacity has zero marginal cost, and the productivity of the asset is determined by the renewable potential in the area. We average both daily solar insolation and daily wind speeds within a location, using data from the Global Solar Atlas and the Global Wind Atlas (as displayed in Figures 2a and 2b). Power generation capacity is extracted from data from the World Resources Institute (see Figure 4).

For the fossil fuel extraction problem, we use data for fossil fuel marginal cost curves from Welsby et al. (2021) for 16 world regions and 3 fuel sources (oil, natural gas, and coal). For each multi-country region we compute the fraction of reserves each country contributes, using the British Petroleum Statistical Review of World Energy (British Petroleum, 2022) and combine the curves of all three

[11] Note that as the regional partition becomes finer, this method of representation will approach the true dataset.

[12] We do this given their similar economics of large fixed costs and variable fuel costs, and not for their role in emitting CO2.

sources by expressing unit costs and production levels in the same energy units, following Clark and Jacks (2007, p. 468).

4.2 Production, Employment, and Trade Data

Our main data source for regional and sectoral value added and employment data is the OECD iLibrary, which includes regional economic and demographic data per year at two different levels of territorial aggregation called territorial levels (TL): TL3 and TL2.[13] The large TL2 regions correspond to political boundaries similar to states. In contrast, smaller TL3 regions, which are contained within in a TL2 region, are similar to counties or commuting zones as discussed above for the US and EU. Whenever possible we aim for TL3 regions, and opt for additional data sources if these are not directly available through OECD. For our calibration we use data for 2015, because in this the latest year where most of the countries had the least amount of missing data by industry. After our selection process and the additions from other datasets we end up with a total of 40 countries and 2506 regions. These regions represent almost 80% of world GDP. We depict the regional and national borders in Figure A5. [14]

To calibrate the trade costs of the model, we measure trade frictions using regional trade data aggregated at the same ten sectors as the gross value added and employment data. The data are based on the EUREGIO Regional Input-Output database (see Thissen et al. (2018)). The survey determines trade flows of different types of goods between regions in Europe and some non-European countries, by surveying all possible modes of transport.[15]

To estimate trade costs, we postulate that they are given by

$$\tau_{ijs} = e^{\omega_s} \left(\mathcal{B}_{inter}\right)^{\mathbb{1}_{C_i \neq C_j}} \left(\mathcal{B}_{intra}\right)^{\mathbb{1}_{i \neq j, C_i = C_j}} \left(d_{ij}\right)^{\beta_s}. \tag{23}$$

with distance d_{ij}, an intra-country border cost, $\left(\mathcal{B}_{intra}\right)^{\mathbb{1}_{i \neq j, c_i = c_j}}$, an inter-country border cost, $\left(\mathcal{B}_{inter}\right)^{\mathbb{1}_{c_i \neq c_j}}$,

[13] We discuss the details of all the construction of the production, employment, and trade data, in our online data appendix.

[14] Sectoral data can be found in https://www.oecd-ilibrary.org/urban-rural-and-regional-development/data/oecd-regional-statistics_region-data-en. The ten ISIC revision 4 sectors we aggregate to in in the data are i. Agriculture, forestry and fishing; ii. Manufacturing, mining and quarrying and other industrial activities; iii. Construction iv. Wholesale and retail trade, transportation and storage, accommodation and food service activities; v. Information and communication; vi. Financial and insurance activities; vii. Real state activities; viii. Professional, scientific, technical, administrative and support service activities; ix. Public administration and defense, education, human health and social work activities; x. Other service activities

[15] These modes include land traffic (by trucks), rail transport, air transport, freight transport, and non-motorized passenger transport.

and a sector-specific cost e^{ω_s}. We then estimate the following gravity regression

$$\begin{aligned}\ln\left(X_{ijs}\right) = &\left(1-\sigma_s\right)\ln\left(\mathcal{B}_{intra}\right)\mathbb{1}_{i\neq j, c_i=c_j} \\ &+\left(1-\sigma_s\right)\ln\left(\mathcal{B}_{inter}\right)\mathbb{1}_{c_i\neq c_j} \\ &+\left(1-\sigma_s\right)\beta_s\ln\left(d_{ij}\right)\mathbb{1}_s+\omega_i+\omega_j+\omega_s+\epsilon_{isj},\end{aligned}$$

where X_{ijs} is the value of the trade flow from region i, sector s, to region j, $\mathbb{1}_s$ is an indicator that takes the value of 1 when the sector is s, $\mathbb{1}_{i\neq j, C_i=C_j}$ is an indicator variable that takes the value of 1 if regions i and j belong to the same country (and are not the same region), $\mathbb{1}_{c_c\neq c_j}$ is an indicator variable that takes the value of 1 if regions i and j belong to different countries, d_{ij} is the distance regions i and j, and ω_i, ω_j, and ω_s are fixed effects for region of origin, destination region, and origin sector, respectively.

The estimates are reported in the Supplementary Material to the paper. We report three salient findings. First, all three coefficients differ across sectors. In particular, the coefficient on log distance shows intuitive deviations from the coefficient of -1 that commonly appears in aggregated gravity regressions (see e.g. Head and Mayer (2014)). The coefficient on construction is -1.34, while the coefficient on information and communication is -0.80. The coefficient on various tradable services (Financial and insurance activities as well as Real state activities/ Professional, scientific, technical, administrative and support service activities) is low, below -0.5. Rerunning the regression aggregated across sectors indeed yields a coefficient very close to -1 (-1.003), and running the regression aggregated across countries for the ten sectors also results in a coefficient much closer to one. Second, the effects of the borders are large. Third, not surprisingly, the inter-country borders affect trade much more than intra-country borders.

4.3 Calibration

We use equation (23) to calibrate the trade costs in the model, τ_{ijs}, using centroid to centroid distances of our regions. We calibrate sectoral trade elasticities using data from Fontagné et al. (2022). We target the employment shares by region-sector and the regional output to calibrate the productivities of the model for each sector, z_{is}, using the full equilibrium structure of the model (Allen and Arkolakis (2014); Redding and Rossi-Hansberg (2017)).

To calibrate factor shares in the final product firms' production function, we use data from the Global Trade Analysis Project (GTAP) global input-output (IO) table, which features 65 sectors in 141 countries. To accommodate our sectoral definitions, we proceed by mapping each of the GTAP sectors to our 10 SNA/ISIC sectors. Using this data, we compute factor shares for fossil fuels, $v_i^{\mathcal{F}}$, for electricity, $v_i^{\mathcal{E}}$, for capital, $v_i^{\mathcal{K}}$, and labor $v_i^{\mathcal{L}}$, by dividing the expenditures on each factor for a given sector-country by the total sectoral expenditures in that country. To obtain total expenditures

in each of these factors, we proceed as follows. For capital and labor, we use factor endowments directly. For fossil fuels and electricity, we label each of the original GTAP sectors as fossil fuels sectors, electricity sectors, or neither. Then, we compute spending from the intermediate input trade data as total expenditure by each sector s in country c on fossil fuel sectors and electricity sectors, respectively.

Recall that ψ is the ease of substituting between direct fossil fuel use and electricity at end use. In a meta-analysis of inter-fuel substitution elasticities in the industrial sector, Stern (2012) finds, in general, elasticities of substitution that are larger than one (though not always significantly so). The cross-sectional meta-elasticities for oil-electricity, gas-electricity and coal-electricity are 2.5, 1.4, and 0.9, respectively.[16] In our baseline calibration we assume $\psi = 1.4$, reflecting the widespread usage of gas in industry.

We specify the production function for energy from fossil capital as

$$Y_j^{\mathcal{F}} = (K_j^{\mathcal{F}})^{\alpha} F_j^{1-\alpha}, \quad Y_j^{\mathcal{F}} \leq \bar{Y}_j^{\mathcal{F},max}.$$

We choose α =0.7 to match a marginal cost curve of fossil fuel electricity that rises slowly with increased power output, matching the slope of marginal cost curves in PJM and other major power markets in the US (see Sahraei-Ardakani et al. (2015)).[17] Maximum output in a region $\bar{Y}_j^{\mathcal{F},max}$ is given by summing the rated capacity of all fossil assets with a region in the data. We use the information on the line length and voltage to construct a value of the resistance for each line in the model by dividing the length (which is measured in centroid to centroid distance if two regions are connected by transmission lines in the data) by the rated voltage in the data. We adjust the overall level of resistances obtained by this procedure on a network to target an initial loss level of 5% (US Energy Information Administration).

To calibrate the learning rate of renewable capital, we begin by using data from the International Renewable Energy Agency (IRENA) on the average total installed cost of wind and solar power. We estimate a regression of the form

$$\log(\text{Total Cost}_t) = a + \gamma \log(\text{Total Installation}_t) + \epsilon_t$$

separately by technology. The results are plotted in Figure (A6), and yield a value of 0.6 for solar and 0.27 for onshore wind. These values are very high compared to the values estimated from micro studies in the literature. The reason is clear: part of the cost declines in renewables are

[16] In particular, these elasticities differ at short and long run horizons, as it indexes the possibility of "electrification". Stern (2012) reports long-run dynamic elasticities, but points out that "none of these elasticities can be estimated with any real precision given the available data." The history of innovation leads us to suspect that long-run substitution elasticities could be substantially higher.

[17] One limitation of this specification is that it is not able to capture sharp increases in marginal cost that are seen when regions are operating at peak output due to the use of gas and oil peaker plants.

due to ongoing research and development and technical progress, and not the economies of scale and learning economies that come from directly increasing output. See Nordhaus (2014) for a discussion. Parameters found in the literature for γ from micro-studies of learning in renewable technologies are typically on the order of $0.1 - 0.25$. However, these studies are mostly unable to account for international or interfirm spillovers. As a compromise, we choose $\gamma_{\mathcal{S}} = 0.35$ and $\gamma_{\mathcal{W}} = 0.2$.[18] Finally, we chose the depreciation rate of knowledge μ to be 1%, reflecting the findings of recent papers estimating very modest rates of forgetting on learning by doing, or none at all (see discussion in Thompson (2010)). We find our quantitative estimates to be mostly unchanged in the presence of higher values of this parameter.

To calibrate renewable potential $\theta_j^{\mathcal{R}}$, we use an estimate of annual kWh/m^2 for solar and wind from the Global Solar Atlas and the Global Wind Atlas. This measure is taken from solar insolation satellite data and wind speed data and combined with assumptions on panel tilt for solar and turbine height for wind, to give potential at a very fine scale of aggregation. We average this measure within each of our regions.

There are four remaining parameters that we externally calibrate. We set the depreciation of renewable capital to 3%, based on the low degradation rates of new renewable photovoltaic and wind turbinesm which are expected to last thirty years or more (Jordan and Kurtz (2013); Wiser and Bolinger (2019)). We set the long run interest rate to be 5%, which determines the discount rate β given that the long-run steady state features no growth.

Lastly, for the fossil fuel module, we allow technology improvements to reduce extraction costs over time. Following the EIA Annual Energy Outlook (U.S. Energy Information Administration, 2022), we impute a 1% year-over-year reduction in marginal costs.

4.4 Model Fit

The model does a reasonable job at reproducing spatial patterns of power prices seen in the data. We collect Locational Marginal Prices for the US from 9 Regional Transmission Organizations, and then average the hourly price at each node in the data for all of 2019. The result is shown in Figure A8, along with the predictions of the model for the equilibrium prices in each region of the US. The states without data do not employ Locational Marginal Pricing and thus cannot be compared to our model predictions.

The higher prices in California and New England are clearly visible. The lower band of prices across the Midwest is also apparent, as are somewhat higher prices in the Rustbelt ex. upstate New

[18] Our quantitative conclusions are very similar in a range of values around these parameters, $\gamma_{\mathcal{S}} \in [0.3, 0.4]$ and $\gamma_{\mathcal{W}} \in [0.15, 0.25]$. As an additional robustness check, we consider exogenous technical progress in capital costs in Section 5.4.

Table 1: OVERVIEW OF PARAMETER CHOICES

	Calibrated Parameters	Value	Source or method
	Global Parameters	Value	Data Source
$\gamma_{\mathcal{S}}$	Learning rate for solar capital	0.35	See text
$\gamma_{\mathcal{W}}$	Learning rate for wind capital	0.2	See text
$\gamma_{\mathcal{B}}$	Learning rate for batteries	0.3	See text
σ_s	Armington elasticities of substitution	Various	Trade elasticities obtained from Fontagné et al. (2022)
α	Curvature on marginal cost of fossil fuel dispatch	0.7	PJM dispatch cost curves for 2020
ψ	E.O.S between electricity and fossil fuels in production	1.4	Stern (2012)
δ^K	Depreciation of physical capital	0.07	Bureau of Economic Analysis, averaging equipment and structures
δ^R	Depreciation of renewable capital	0.03	See text
δ^F	Depreciation of fossil capital	0.02	Bureau of Economic Analysis
v^l_{js}	Production function coefficients	Various	Factor shares by country and sector from the Global Trade Analysis Project
ϱ	Frechet dispersion for renewable project shifters	0.7	Match wind and solar split in 2021
	Fossil Extraction	Value	Data Source
$\xi(q)_c$	Fossil Fuel Marginal Cost	Various	Welsby et al. (2021)
$g^{\mathcal{F}}$	Rate of improvement in fossil extraction cost	0.01	U.S. Energy Information Administration
	Local Fundamentals	Value	Data Source
z_{js}	Local sectoral productivity	Various	Matching local wage and employment data
τ_{is}	Sectoral trade costs between i and j	Various	EUREGIO Regional Input-Output database, gravity regression
$\Omega^{\mathcal{R}}_j$	Regional shifter of investment costs	Various	International Renewable Energy Agency Cost Database
	Grid Fundamentals	Value	Data Source
θ_j	Renewable Potential	Various	Satellite data on Mwh/m^2 solar and wind potential
$\mathbf{R}$	Line resistance matrix	Various	Open Street Map
$\mathbf{A}$	Line adjacency matrix	Various	Open Street Map
$\mathbf{Z}^{max}$	Maximum Line Capacity	Various	Open Street Map and author calculations

Notes: This table shows the baseline parameterization of the model, as well as the sources and moments used to calibrate the model.

York. Some notable misses of the model include the West Texas oil fields (the dark crimson areas of Texas), which are huge consumers of electricity, and have no analogue in the model. Overall, the model can reproduce fairly well the variation in spatial prices in at least one region of the world for which we have data.

4.5 Extensions for Quantitative Analysis

We now introduce two extensions to the baseline model that can partially address the intermittency of renewables indirectly, as we have sidestepped modeling their stochastic nature. In particular, in line with the discussion in Baker et al. (2013), we model backup batteries requirements and overbuilding for renewables.[19]

Batteries. We assume every unit of renewable capital must be paired with a battery of size B, where size is measured in MWh. These sizes we consider are 0, 2, 4 and 8 MWh per each unit of renewable capital (recall that size is measured in MW). Batteries are produced under constant returns, and available at price $p^{\mathcal{B}}_{j,t}$, where $p^{\mathcal{B}}_{j,t}$ follows a learning process similar to that of renewable capital, given by

$$p^{\mathcal{B}}_{j,t} = \left(\sum_{j'} \sum_{i=1}^{\infty} (\mu)^i Q^{\mathcal{B}}_{j',t-i} \right)^{-\gamma_{\mathcal{B}}} P^{\mathcal{C}}_{j,t}. \tag{24}$$

where $Q^{\mathcal{B}}_{j',t-i}$ is the quantity of batteries produced. We take the learning rate for batteries $\gamma_{\mathcal{B}}$ to be $\gamma_{\mathcal{B}} = 0.35$, roughly in line with estimates from the literature, and reflecting somewhat slower expected price declines with output than in the recent past, due to projected supply constraints for battery materials.

Overbuilding and Curtailment. Additionally, we consider the idea that one way of dealing with the intermittency of renewables is to simply build more capacity than is generally needed, so that in times of low wind speeds or sunlight, the extra capacity can compensate. In normal times, surplus electricity is curtailed, or wasted, and generators are not paid for this lost output. .This effectively resembles a lower purchase price of renewable energy recently observed in markets with excess renewable capacity as pointed out by Das et al. (2020). Even with significant curtailment, positive investment can still be profitable for investors as long as renewable capital prices fall far enough. See Section 5.3 for more details.

[19] As the authors point out, for solar renewables "intermittency of a solar resource can add to system costs, as additional system reserves and backup generation may be required to maintain system reliability". The remaining unmodeled complication that intermittency brings is the covariance of demand and yield of renewables, for example high output of photovoltaic when energy is needed for cooling in the summer and low energy output in the winter when energy is needed for heating, as is considered in Lamont (2008); Baker et al. (2013). Our model can be simulated at high frequency to incorporate those effects of seasonal intermittency, an extension we leave for future research.

5 Clean Growth Scenarios

In this section, we assess the impact of renewable energy on income growth, prices and welfare. We solve for a perfect foresight equilibrium, beginning with the calibrated model in 2020, and shooting forward until the model reaches a new steady state. We then consider the extensions outlined above, before finally turning to policy.

5.1 Clean Growth Across the Globe

We begin by examining the long run consequences of the energy revolution. In Figure 5 we plot the changes in per-capita annual welfare across countries induced by the energy transition, comparing future years to the outcomes at the beginning of the transitional dynamics (in 2021). We decompose welfare changes into several informative components, and define the change in welfare as the change in real expenditure per-capita:

$$dlnW_j = dln(E_j/P_j),$$

where

$$dln(\frac{E_j}{P_j}) \approx \underbrace{dln(\frac{w_j}{P_j})\frac{w_j L_j}{E_j}}_{\text{real wage changes}} + \underbrace{dln(\frac{r_j^{\mathcal{K}} k_j}{P_j})\frac{r_j^{\mathcal{K}} k_j}{E_j}}_{\text{capital deepening}} + \underbrace{dln(\frac{\Xi_j}{P_j})\frac{\Xi_j}{E_j}}_{\text{electricity sales growth}} + \underbrace{dln(\frac{\Pi_j^{\mathcal{F}}}{P_j})\frac{\Pi_j^{\mathcal{F}}}{E_j}}_{\text{loss of fossil profits}}, \tag{25}$$

and where $\Xi_j \equiv p^{\mathcal{E}} Y_j^{\mathcal{E}} - p^{\mathcal{F}} F_j^{\mathcal{E}} + \Pi_j^{\mathcal{E}}$ is net electricity sales revenue. In the long-run, adoption of renewable capital can have four primary effects. First, growth of renewables results in lower prices and induces changes in specialization across industries. This can cause real wage gains through aggregate price index declines, but also some regions to become relatively more well off compared to others through terms of trade effects. Second, cheaper electricity induces capital deepening, raising output. Third, electricity sales grow as more renewable capital is installed, and industry is electrified. Lastly, countries which are currently exporting fossil fuels lose this revenue in the long run.

To plot this at the country level, we take the weighted average of welfare changes for regions within a country, and show this in Figure 5. Welfare gains are large. The average welfare gain by 2040 is 4.6%, though is this very heterogeneous across regions. For a point of reference, Cruz and Rossi-Hansberg (2021) estimate the costs of long run climate change in the high emissions scenario of 5.1 degrees of warming by 2100 as 6%, and for 2.9 degrees as 1%. As such, the pure economic benefits of technologies designed to alter the warming path of the world are of a similar order to the detrimental effects of climate change in a business as usual, high emission scenario. Results for

Figure 5: Welfare Changes to 2040

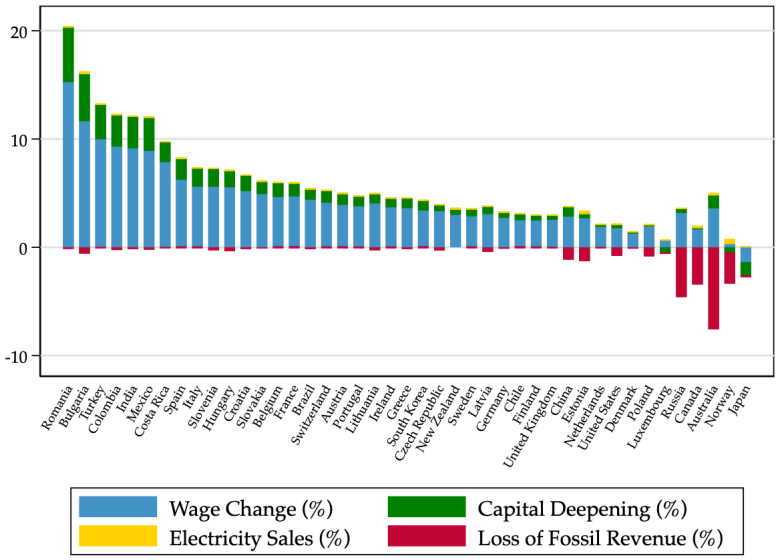

Notes: This Figure shows the welfare changes in by 2040 at the country level. Welfare changes across regions are aggregated to the country level via an employment weighted average. The decomposition of these changes is computed according to equation (25).

the long run steady state are shown in Figure (A10), where the average welfare gain rises to 7.3%. Countries that benefit most tend to have high renewable potential and/or initially high electricity costs. Importantly, a set of fossil-fuel exporting countries (Australia, Russia, Canada and Norway) lose on net from the energy transition, primarily due to losses in fossil-fuel export revenue.

Indeed, the gains from the renewable energy transition are even larger than is apparent here. An important factor dampening the long-run welfare gains is that in the long-run steady state of the model, fossil fuels have been completely exhausted. This loss of a factor of production is only partially ameliorated by electrification of industry, since we assume the elasticity of substitution ψ is relatively low at 1.4. The loss of economically useful fossil fuels depresses the welfare gains of the clean energy transition in a way that is not immediately apparent from Figure 5. While fossil fuel exporters suffer disproportionately from the loss in fossil revenue, all countries are hurt by an increase in the price index from phasing out fossil fuels.

Figure 6 presents an aggregate summary of the energy transition transitional dynamics. The model predicts that the aggregate price of solar capital falls by over 50% by 2040. While substantial, this is somewhat lower than the previous pace of price declines seen for solar, and consistent with projections from SETO (2021). As seen in Figure A6, in the previous decade (from 2010 to 2020), the total installed price of solar capital decreased by 81%. The reason is twofold. Once capital becomes widely adopted in many regions, passing the initial threshold of no investment, proportional increases in the total stock installed worldwide begin to slow (though the learning rate γ remains unchanged). Second, we have taken a somewhat lower learning rate for renewable capital than

Figure 6: Renewable Transition Path

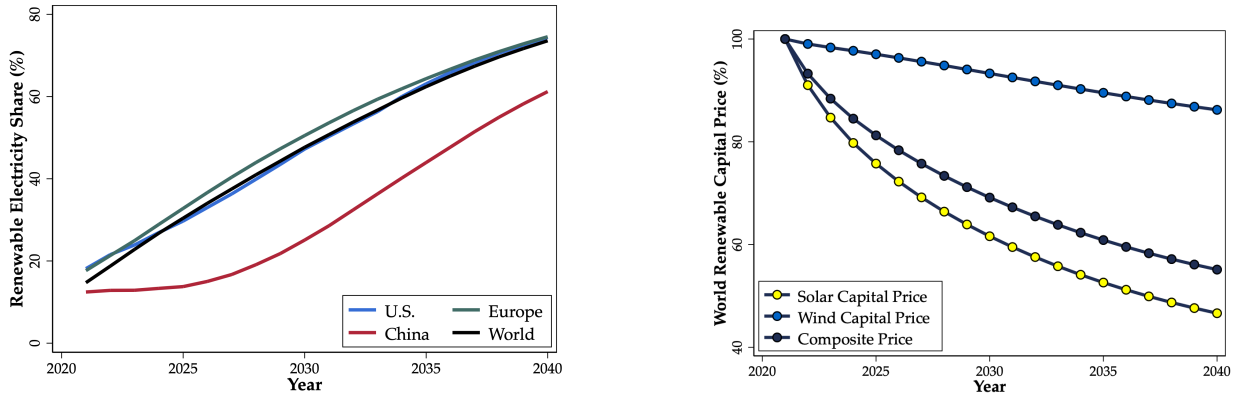

The left panel shows the share of electricity coming from renewables in each country or region in the baseline scenario. This right panel shows the model's projection for the world capital prices in the baseline scenario, normalized to 100 in 2021.

is observed in the data for both solar cost and wind. The pace of the projected decline for wind capital prices is substantially slower than for solar, owing both to the lower learning rate and to the fact that the renewable mix shifts continually toward solar, as the solar price drops faster than the wind price.

Most countries around the world achieve substantial renewable energy shares by 2040. The US and Europe rise to over 70% renewable power by 2040 on the basis of capital cost declines alone. China takes much longer, owing to an abundance of fossil fuel capital and relatively cheap power prices, which discourages the initial take up of renewables.

It is worth emphasizing that this is not a forecast, but a quantitative illustration of the cost effect of learning-based capital price declines on the world energy system. Still, several features of reality have been abstracted from that may quantitatively shape the transition. In particular, this is a frictionless investment model. In reality, there may be congestion effects in the construction sector that impede the ability of countries to install the amount of capital projected here. In addition, while line constraints are modeled in detail, there are technical limitations due to temporal mismatches of renewable supply and energy demand, which may become more severe with greater renewable penetration. This intermittent nature of renewables means that substantial backup is likely to be necessary, and we now consider the role of battery storage in providing this backup.

5.2 Batteries

To set the initial level of battery costs, we use the current price of a Tesla Megapack. Currently available in modular units of 3.9 mWh and 1.9 MW power output, these packs are widely use

Figure 7: Renewable Transition Paths Under Battery Scenarios

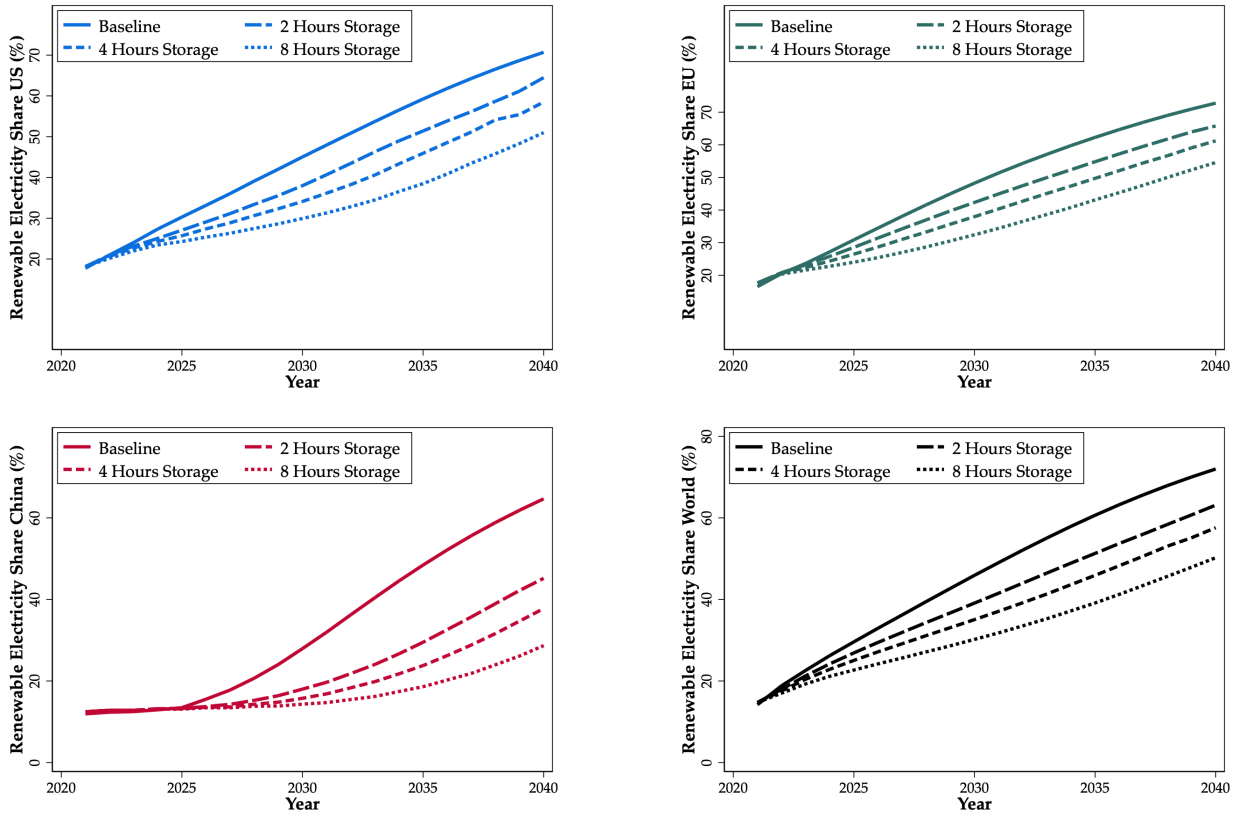

Notes: This figure plots the share of electricity by country coming from renewable sources in four different scenarios: the baseline, without any storage requirements, and then 3 scenarios of storage pairing with renewable capital.

Figure 8: Capital Prices under Battery Scenarios

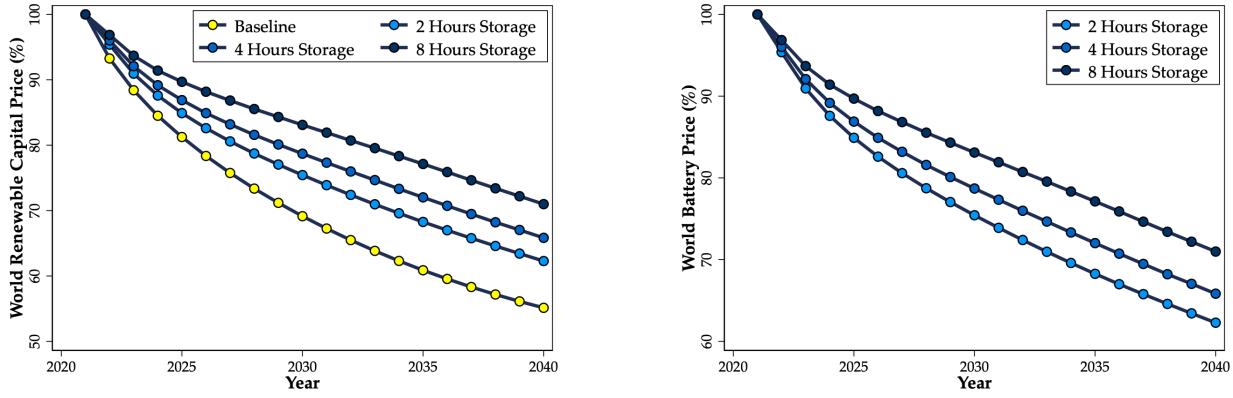

Notes: The left panel shows the composite renewable capital price under different battery scenarios. The right panel shows the bath for battery prices under different battery scenarios.

in nascent battery projects across the world.[20] As of the time writing, this cost works out to be $482 per kWh. We then let the price of batteries evolve along the transition according to the law of motion in equation (24). Recall that we require that each unit of renewable capital must be paired with a battery of size h, so that the free entry condition now becomes

$$(\bar{P}_{j,t} + hp^{\mathcal{B}}_{j,t}) \geq R_t^{-1}\left(p^{\mathcal{E}}_{j,t+1}\bar{\theta}_{j,t} + (1-\delta)\bar{P}_{j,t+1} + (1-\delta^{\mathcal{B}})hp^{\mathcal{B}}_{j,t+1})\right),$$

where again $\bar{P}_{j,t}$ is the expected price of the renewable mix in region j at time t. We set the depreciation rate of batteries, δ^B, to 0.05, reflecting an expected lifetime of 20 years.[21] The learning rate γ_B is set to 0.35, reflecting a conservative discount of the rate in Figure A7. The results for the transition paths are plotted in Figure 7. In each region, requiring the adoption of batteries moderately slows renewable penetration out to 2040. However, even in the most restrictive scenario, the world still reaches 50% renewable penetration by 2040. Ongoing capital price falls for batteries with continued uptake gradually allow renewables to dominate most areas of the grid.

We also note that mandating a larger battery market from the beginning actually does not lead to cheaper battery prices through learning by doing, as we show in Figure 8. The increased costs from mandating larger amounts of storage act as a deterrent to renewable adoption, which leads to *less* battery adoption in equilibrium. In the 4 hours and 8 hours of storage scenarios, battery prices decline significantly slower than the 2 hours scenario.

5.3 Curtailment and Overbuilding

But how much battery storage is actually required? To begin to answer this, we introduce curtailment into the model. The problem of renewable intermittency leads at time to excess energy generation which, without substantial storage, results in curtailment. We incorporate estimates of curtailment modeled as efficiency loses in electricity generation of renewables using the measurements of Shaner et al. (2018) and Tong et al. (2021). The authors measure curtailment using precise geophysical measures of solar and wind potential and demand of countries, as well as various other geophysical constraints such as spatial variability, transmission network, and demand fluctuations. In particular, Tong et al. (2021), do so under various battery storage scenarios for 18 major countries.

We take advantage of their estimates to construct a continuous measure of curtailment of wind and solar production as a function of penetration of each of the resources and different battery storage scenarios. We use the estimates of Tong et al. (2021) for 17 countries to calibrate curtailment factors for each country in our dataset.[22] Details are provided in Appendix A3. We illustrate

[20] See, for example, the Hornsdale Power reserve, which was the world's first large scale battery installation in 2017, and more recently the Moss Landing substation for PG&E in California.

[21] For example, the current warranty on a Tesla Megapack is for 20 years.

[22] We apply the US estimates for the US and any country that the authors do not provide estimates for

Figure 9: Considering Curtailment and Overbuilding in the Renewables Transition

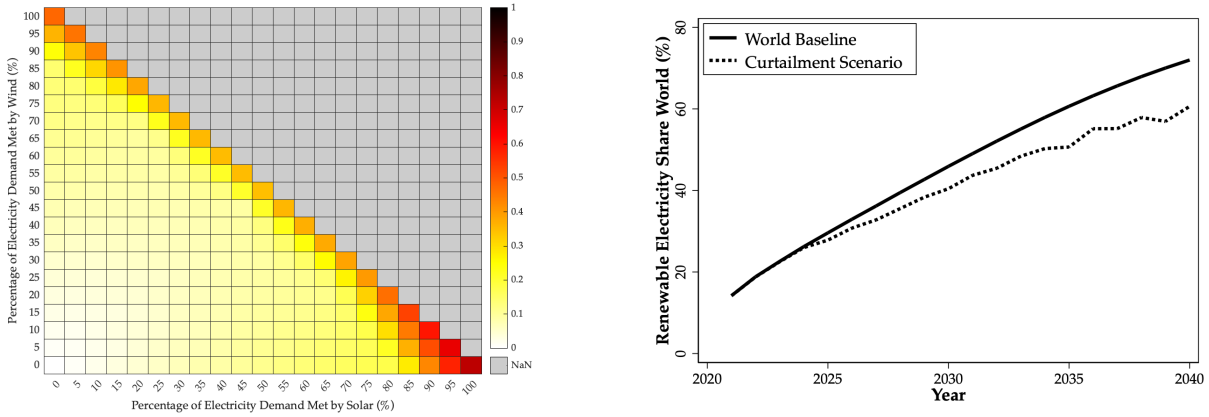

Notes: The left panel shows curtailment as a function of wind and solar penetration in the country with 12 hours of storage on the grid. The right the share of electricity coming from renewables at the world level in the baseline scenario and under after incorporating curtailment.

the US curtailment estimates in the left panel of Figure 9. For example, with 12 hours of storage, if solar energy capacity is 30% of the nominal demand and wind 30% of the nominal demand, then curtailment is about 15% over a year. But if instead 85% of electricity is produced by solar with 15% wind contribution, then curtailment is more severe, on the order of 40%. Curtailment ameliorates substantially the more battery storage is introduced. In Figure A11 in the Appendix we plot the same figure for 4 hours and 0 hours of storage. Note also that wind and solar are somewhat complementary; a fully wind-based grid loses around 50% of energy generated (or equivalently overbuild of generating capital of 100%), whereas a 50-50 wind and solar mix loses around 30% of energy in a scenario of 12 hours of storage. A 100% solar grid loses a substantial amount of energy even with 12 hours of storage, requiring a very large overbuild of generating capital.

We model curtailment as reducing the amount of output from both solar and wind capital by the endogenous fraction $C_{j,t}$, using the estimates described above, such that the free entry price in any period is

$$(\bar{P}_{j,t} + h_{j,t} p^{\mathcal{B}}_{j,t}) \geq R_t^{-1} \left(p^{\mathcal{E}}_{j,t+1} \bar{\theta}_{j,t} C_{j,t} + (1-\delta) \bar{P}_{j,t+1} + (1-\delta^{\mathcal{B}}) h_{j,t} p^{\mathcal{B}}_{j,t+1}) \right).$$

The fraction $C_{j,t}$ is determined at the grid level, and is taken as exogenous by investors in any region j. In addition, we now make battery storage requirements $h_{j,t}$ a function of overall renewable penetration on the grid. To do so, we adopt a "worst-case" storage requirement by total renewable penetration which keeps maximum curtailment losses below 50%. Due to data limitations, we cap the maximum amount of battery storage at 12 hours. This storage requirement is plotted in Figure A12 for illustrative countries. Battery storage is not required for low levels of renewable penetration, before rising sharply once total penetration reaches 50-60%.

This scenario only slightly slows world progress out to 2040, as shown in the right panel of Figure

Figure 10: Renewable Transition Paths under Exogenous Technical Progress

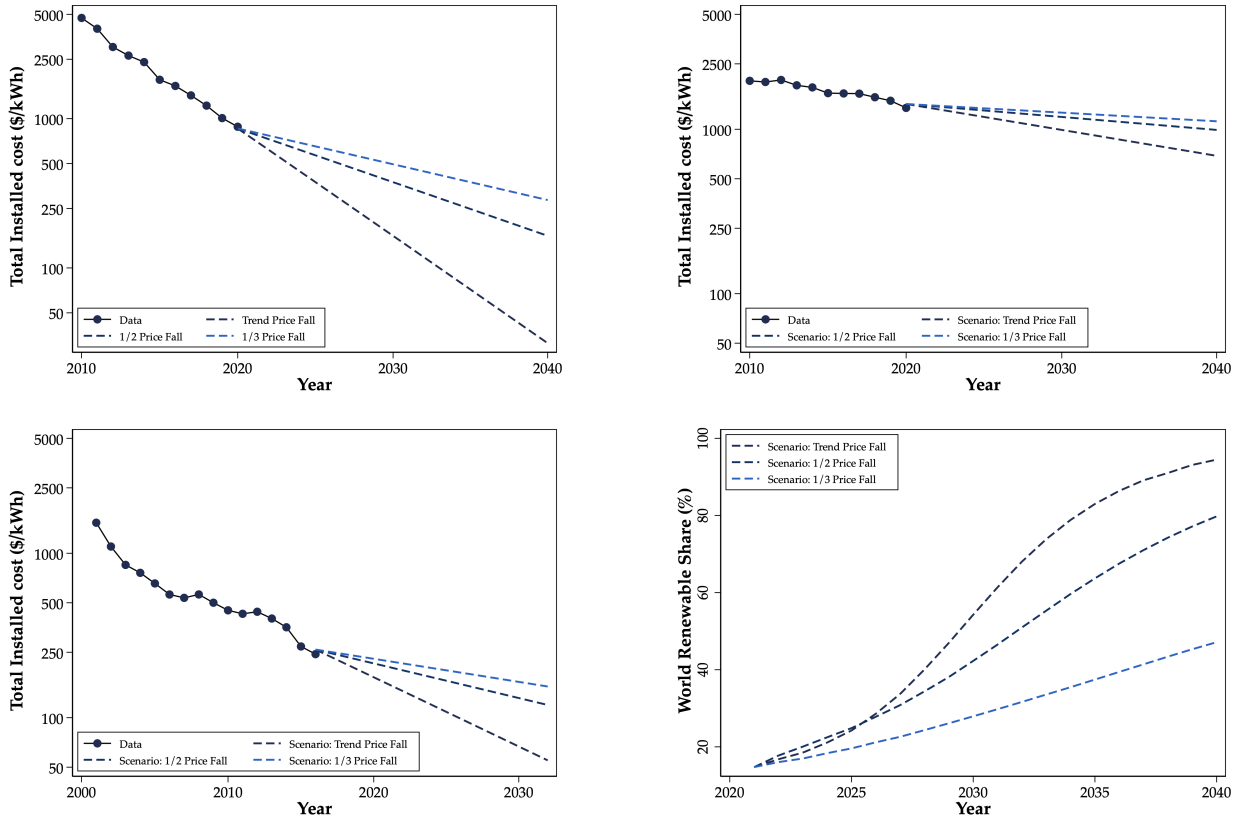

Notes: The top left panel shows projections for the cost of solar capital, and the right for wind, using historical data from IRENA in constant $2019. The bottom left panel shows the same for batteries using data from Ziegler and Trancik (2021b), available from Ziegler and Trancik (2021a). The bottom right shows projections for the world renewable share under these different scenarios.

9. Both curtailment and battery storage requirements are mild almost everywhere for at least a decade, enabling rapid initial cost falls in renewable capital prices. These frictions only begin to have a quantitative effect in the late 2030s.

5.4 Robustness with Exogenous Technical Progress

The results in this paper are somewhat sensitive to the specification of the learning rates γ_S and γ_W, and speculation whether the aggregate rate is stable and will remain at its current value for the foreseeable future is reasonable. Though price declines in solar in particular have been more or less constant for 50 years, this is is no guarantee that they will continue in this manner. As a robustness exercise, in this section we consider what the path for the renewable transition would look like under different assumptions about exogenous technical progress, with no learning by doing.

To do so, we estimate a linear trend for solar and wind capital costs off the last ten years of data, and then extrapolate this trend out to 2040, attributing previous prices falls to exogenous technical

progress. Beyond 2040, we assume technical progress stops. We consider a case where the trendline remains the same, and also scenarios where the speed of improvement slows by 50% and two thirds. The results are shown in Figure 10. We find that at current rates of technical progress in these technologies, the world energy system transitions to renewables even faster than our baseline scenario with endogenous capital price falls. Even a significant slowing of these trends imply a fairly rapid decarbonization. We thus view our specification of the learning rates in the baseline as a mildly conservative assumption.

5.5 Discussion

There are three salient lessons that emerge from this analysis.

First, absent other forces, the world is likely to shift to renewable energy quickly in the coming decades, even when we incorporate realistic scenarios for battery storage requirements and curtailment. If renewable capital prices continue to fall at anything like the pace they have in recent times, renewable dominance is ineluctable.

Second, the combination of technical progress in capital build and zero marginal cost of generation exerts heavy downward pressure on power prices, leading to substantial welfare gains. Most countries and regions stand to benefit from the renewable transition, though relatively large losses are in store for fossil fuel exporters as the world electrifies and winds down its fossil generating capital.

Third, current grid structures do not hinder the uptake of renewable energy. A significant advance in this study relative to prior work is the ability to model seriously the capacity limitations of the current electricity grid at a detailed level. Despite the fact that productive renewable resources and demand tend to be spatially mismatched, and capacity for transfer of power across space is limited, the renewable transition is swift. The reason is that renewable capital is modular. Power generation can be built in any size, from small installations to mega-projects, without substantial changes in the levelized cost of a unit of energy. This makes it relatively easy to site renewable generation locally in the amount required. In the model, the dominant factor driving installation is not renewable potential, but falling capital costs. Once capital gets cheap enough, it makes sense to install solar panels and batteries in Maine. This is not to say that grid investment cannot yield substantial welfare gains (see below), only that the current grid structure is not inimical to clean growth.

6 Clean Policies

6.1 The Inflation Reduction Act and Renewable Subsidies

We now turn to policy, and study the effects of a subsidy in the form of a production credit to renewable energy. In August 2022, the Biden Administration signed into law the Inflation Reduction Act, which contained significant spending measures designed to encourage the uptake of renewable energy. Chief among these was an production tax credit of $26 per MWh for renewable energy from any source, extended out to 2033 (H.R.5376 - Inflation Reduction Act of 2022). Certain domestic labor and materials are required to receive the full credit, and if they are not met, then the credit is reduced to $5.

We model this by assuming that electricity produced for renewable sources receives a subsidy s_t, so that

$$\bar{P}^{\mathcal{R}}_{j,t} \geq R_t^{-1}\left((p^{\mathcal{E}}_{j,t} + s_t)\bar{\theta}_{j,t} + (1-\delta)\bar{P}^{\mathcal{R}}_{j,t+1}\right).$$

The subsidy is funded by labor income taxes on all regions in the US, with a time varying (but spatially invariant) rate τ_t, which solves

$$\sum_{j \in US} w_{j,t} L_j (1 - \tau_t) = s_t \sum_{j \in US} Y^{\mathcal{E}}_j.$$

There are no taxes in the model, and thus directly comparing this to the electricity revenue received by a unit of renewable capital is not immediate. We proceed as follows. We first note that $5 is around 15% of the average wholesale price prevailing in markets with locational market prices in 2020, and set the value of s_t in the model to be 15% of the average equilibrium 2020 $p^{\mathcal{E}}_t$ in the US.[23] We assume that the subsidy is removed after 2032, and goes to zero in 2033. We solve for the counterfactual global equilibrium, holding all other regional fundamentals constant.

The results are presented in Figure 11. The production tax credit induces significant uptake of renewable energy in the US over and above the baseline case. Instead of reaching 45% of electricity production by 2030, the renewable share is 57%. The gap between the baseline and counterfactual renewable share then closes as the credit is withdrawn, and in the long run has no permanent effect. Again, it is worth emphasizing that this is not a forecast, given the abstractions we have made out of necessity, but instead is an illustration of the power of existing renewable subsidies to speed up the energy transition.

It is also worth noting that in this model, the IRA production credit can have only transitional effects. This is due to the forgetting rate μ, which discounts production in the far past in affecting

[23] It is difficult to ascertain from a reading of the bill just how restrictive the conditions are to receive the full $26. We thus model the effects of the lower amount.

Figure 11: The Impact of the Inflation Reduction Act

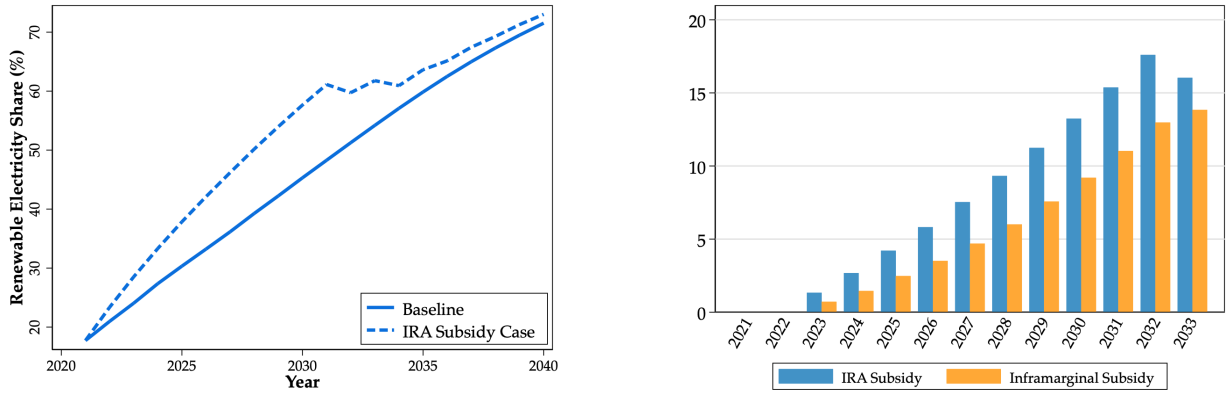

Notes: The top left panel shows the model's projection for renewable power share under the IRA production tax credit, and without. The top right panel shows the total cost of the bill (in blue), and subsidies going to capital that would be installed in the absence of the subsidy. The bottom left shows GDP growth in both scenarios, and the bottom right shows the renewable capital price.

the price of capital today. As such, the IRA cannot effect the long run steady of the model, as infinitely far into the future its effects have been lost. It only has transitional effects, speeding up adoption in the movement towards the long run steady state.

The credit goes some way to accelerating world-wide adoption, modestly increasing adoption in other countries. This is because the US is a substantial buyer of renewable capital on the world market, and accelerating adoption plans domestically increases world production of capital, thereby putting downward pressure on the price via learning by doing. By 2030, the world renewable capital price is 7% lower thanks to the IRA than it would be in the baseline with no subsidies.

The budgetary costs of the IRA are substantial, but within the projections of the bill itself. The IRA bill budgets for $160 billion in spending on the production tax credit. We find instead that around $104 billion is spent before the subsidy expires in 2034. Over 70% of this total goes to subsidizing inframarginal investment, or investment that would have happened absent the subsidy. This is due to the relatively rapid adoption in the baseline case; much of the renewable transition appears likely on the basis of cost declines alone.

However, the intervention more than pays for itself. We find that the the intervention generates around $970bn of additional GDP on the transition, due to cheaper power prices both in the US and around the world. This more than justifies the budgetary outlay. The reason is simple: dynamically, the world economy is not efficient, since firms do not internalize the cost benefits for other future capital producers when they expand output. Note also that this figure does not take into account any additional benefits of carbon reduction, nor does it consider the spillover effects onto the GDP of other countries.

These conclusions are robust to incorporating curtailment and battery storage, as in Section 5. For

Figure 12: Proposed US Grid Improvements

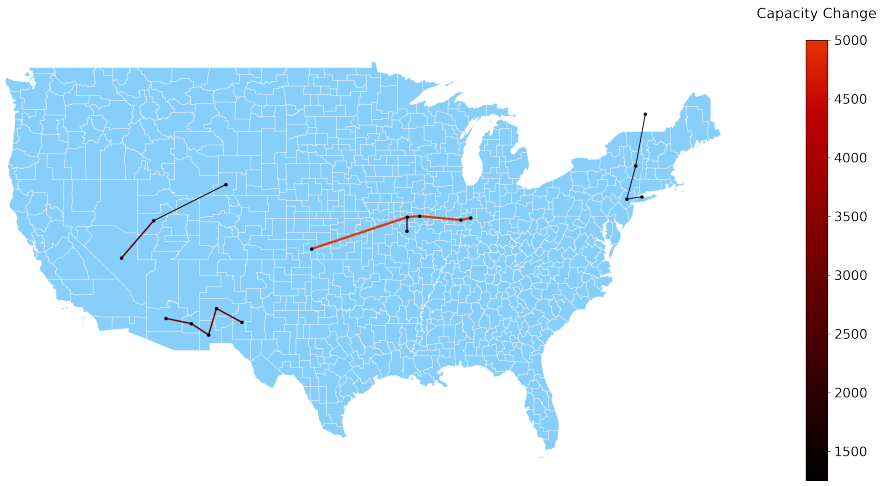

Notes: This figure shows our representation of four large-scale transmission projects proposed for the US. Colour and thickness of lines corresponds to capacity (in MW). More detail on line construction is given in the replication guide for this paper.

curtailment, since battery storage requirements do not begin to endogenously bite until the late 2030s, the initial equilibrium path under subsidies is virtually unchanged to that presented here. If instead we require by fiat battery storage now for each unit of renewable capital, as in Section 5.2, the adoption path shifts downwards, but the additional uptake induced by the IRA over the no subsidy case is similar. An example is presented for 4 hours of storage in Figure A13.

6.2 Grid Improvements

In this final section, we consider the benefits of grid improvements. We do so by integrating four large-scale grid enhancements currently under construction in the US into our representation of the US grid. First is the Champlain-Hudson Power Express line, which aims to connect Queens and New York City to Quebec with 1250 MW of capacity. Second is the Grain Belt Express line, a 5GW capacity line connecting Illinois to Missouri and Kansas. Third is the Sun Zia Transmission line, a 3GW line between Arizona and New Mexico. Last is the TransWest Express line, which runs from Wyoming to Las Vegas with 3GW of capacity. We show these in Figure 12. Together, these lines are estimated to cost around $10 billion in upfront construction cost.

We assess the benefits of these new lines by re-solving the long run steady state with the improved grid. Several key results are important. First, the majority of prices do not change in the new steady state. This is because in most regions, the model infers that the free entry condition holds with equality in the long run. Examining equation (22), if global capital prices are unaffected by small investments, and local price shifters do not change, then the local price of energy is similarly unaffected. It is only in regions where the energy price is below the free entry cutoff (and hence

Figure 13: Counterfactual Electricity Price Changes

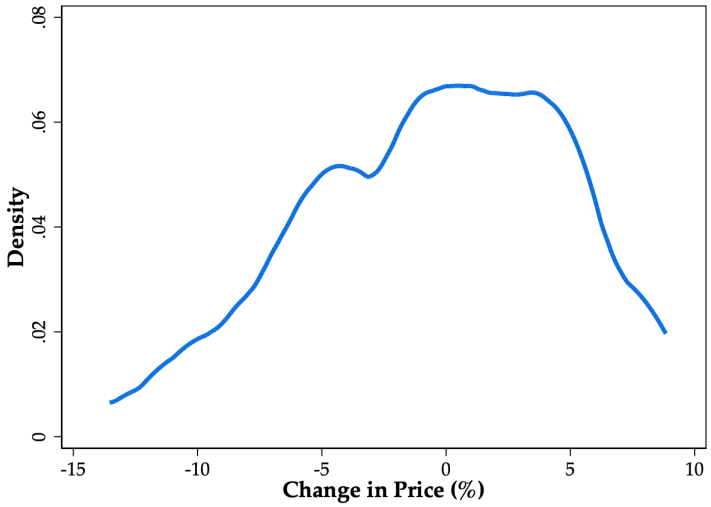

Notes: This figure shows an estimate of the distribution of price changes under the proposed grid improvements. Price changes of zero have been omitted from the figure.

which host zero generation capacity), that grid investment can have an effect on long run power prices.

Second, the investment does not uniformly lower prices in the regions below the free entry cutoff. We show in Figure 13 the estimated price changes. A number of regions actually experience price *increases*. The reason has to do with the equation for locational marginal prices in (14). The congestion component in region j depends on the Lagrange multiplier on each constrained line, multiplied by whether extra load in node j would increase or decrease power flow on that line. As the Lagrange multiplier falls on lines which expand capacity, this can have a positive or negative effect on local power prices.

Third, the expected benefit of these lines is substantial, generating an additional $1.5 billion in annual GDP once completed. While we do not explicitly model discounted costs and benefits on the transition owing to uncertainty in the timeline of each upgrade's rollout, under a wide range of assumptions this would more than justify the construction cost of the lines. This hints at the potential of transmission improvements and grid upgrades in a world of high renewable penetration.

7 Conclusions

We have developed a spatial theory of clean growth to assess the global rise of renewable energy. We find that continued growth in renewable installation is likely to lead to substantial falls in the

price of power, with widespread benefits for production and real wages. Most countries benefit from this technological shift, though the long run effect depends on initial power prices and the strength of the transmission networks. Production based subsidies of the kind seen in the US with the Inflation Reduction Act of 2022 can substantially accelerate the renewable energy transition.

We see a number of avenues for future research. First, our approach does not distinguish between scale effects led by technological innovation or learning spillovers. Subsidies on innovation or scale would differentially affect growth outcomes under these different scenarios, and more research is needed to understand the effects of such policies. Second, we think it is important to evaluate the labor market effects of the growth of the renewable sector, given the comparative advantage of different regions and its rapid growth (see (Hanson, 2023)). Third, much work remains to do on how to plan optimal grid investment. Our approach evaluates specific proposed projects, but the analysis of how these infrastructure improvements can be optimally designed raises important methodological challenges.[24] These challenges are at the forefront of the agenda for climate policy.

References

Acemoglu, Daron, Philippe Aghion, and David Hémous, "The Environment and Directed Technical Change in a North–South Model," *Oxford Review of Economic Policy*, 2014, *30* (3), 513–530. [5]

_ , _ , Leonardo Bursztyn, and David Hemous, "The Environment and Directed Technical Change," *American Economic Review*, 2012, *102* (1), 131–166. [5]

Allcott, Hunt, Allan Collard-Wexler, and Stephen D O'Connell, "How do Electricity Shortages Affect industry? Evidence from India," *American Economic Review*, 2016, *106* (3), 587–624. [5]

Allen, Treb and Costas Arkolakis, "Trade and the Topography of the Spatial Economy," *The Quarterly Journal of Economics*, 2014, *129* (3), 1085–1140. [4, 22]

Alvarez, Jose Luis Cruz and Esteban Rossi-Hansberg, "The economic geography of global warming," Technical Report, National Bureau of Economic Research 2021. [4]

Anderson, James E., "A Theoretical Foundation for the Gravity Equation," *American Economic Review*, 1979, *69* (1), 106–116. [1]

Arkolakis, Costas, Fabian Eckert, and Shi Rowan, "Combinatorial Discrete Choice: A Quantitative Model of Multinational Location Decision," *Available at SSRN 3455353*, 2017. [39]

Armington, Paul S., "A Theory of Demand for Products Distinguished by Place of Production," *International Monetary Fund Staff Papers*, 1969, *16*, 159–178. [1, 12]

[24] In particular, a naive formulation of the line investment problem takes the form of "combinatorial discrete choice" (Arkolakis et al., 2017), a class of problems for which the choice space is so large as to render standard methods infeasible.

Asker, John, Allan Collard-Wexler, and Jan De Loecker, "(Mis) allocation, Market power, and Global oil extraction," *American Economic Review*, 2019, *109* (4), 1568–1615. [4]

Australian Energy Market Commission, "Transmission Access Reform: Updated Technical Specifications and Cost-Benefit Analysis," *Interim Report*, 2020. [15]

Baker, Erin, Meredith Fowlie, Derek Lemoine, and Stanley S Reynolds, "The Economics of Solar Electricity," *Annu. Rev. Resour. Econ.*, 2013, *5* (1), 387–426. [1, 4, 17, 26]

Benkard, C Lanier, "Learning and Forgetting: The Dynamics of Aircraft Production," *American Economic Review*, 2000, *90* (4), 1034–1054. [16]

Benthem, Arthur Van, Kenneth Gillingham, and James Sweeney, "Learning-by-doing and the Optimal Solar Policy in California," *The Energy Journal*, 2008, *29* (3). [1]

Bohn, Roger E, Michael C Caramanis, and Fred C Schweppe, "Optimal Pricing in Electrical Networks Over Space and Time," *The Rand Journal of Economics*, 1984, pp. 360–376. [9, A13]

Bohringer, Christoph and Andreas Loschel, "Promoting Renewable Energy in Europe: A Hybrid Computable General Equilibrium Approach," *The Energy Journal*, 2006, (Special Issue# 2). [4]

British Petroleum, "Statistical Review of World Energy," Technical Report, British Petroleum 2022. [20]

Clark, Gregory and David Jacks, "Coal and the Industrial Revolution, 1700–1869," *European Review of Economic History*, 2007, *11* (1), 39–72. [17, 21]

Clo, Stefano, Alessandra Cataldi, and Pietro Zoppoli, "The Merit Order Effect in the Italian Power Market: The Impact of Solar and Wind Generation on National Wholesale Electricity Prices," *Energy Policy*, 2015, *77*, 79–88. [8]

Colmer, J, D Lagakos, and M Shu, "Is the Electricity Sector a Weak Link in Development?," *Working Paper*, 2023. [5]

Conte, Bruno, Klaus Desmet, Dávid Krisztián Nagy, and Esteban Rossi-Hansberg, "Local Sectoral Specialization in a Warming World," *Journal of Economic Geography*, 2021, *21* (4), 493–530. [4]

Costinot, Arnaud and Andrés Rodríguez-Clare, "Trade Theory with Numbers: Quantifying the Consequences of Globalization," in "Handbook of international economics," Vol. 4, Elsevier, 2014, pp. 197–261. [4]

Covert, Thomas, Michael Greenstone, and Christopher R Knittel, "Will We Ever Stop Using Fossil Fuels?," *Journal of Economic Perspectives*, 2016, *30* (1), 117–138. [19]

Cretì, Anna and Fulvio Fontini, *Economics of Electricity: Markets, Competition and Rules*, Cambridge University Press, 2019. [9]

Cruz, José-Luis and Esteban Rossi-Hansberg, "The Economic Geography of Global Warming," Technical Report, National Bureau of Economic Research 2021. [27]

Das, Saptarshi, Eric Hittinger, and Eric Williams, "Learning is Not enough: Diminishing Marginal Revenues and Increasing Abatement Costs of Wind and Solar," *Renewable Energy*, 2020, *156*, 634–644. [26]

Decker, Christopher, "Energy Transportation: Electricity," in "Handbook of Energy Economics and Policy," Elsevier, 2021, pp. 193–238. [8, 14]

Edenhofer, Ottmar, Lion Hirth, Brigitte Knopf, Michael Pahle, Steffen Schlömer, Eva Schmid, and Falko Ueckerdt, "On the Economics of Renewable Energy Sources," *Energy Economics*, 2013, *40*, S12–S23. [5]

European Network of Transmission System Operators for Electricity, "Report on the Locational Marginal Pricing Study of the Bidding Zone Review Process," *Report*, 2022. [15]

Fiszbein, Martin, Jeanne Lafortune, Ethan G Lewis, and José Tessada, "Powering Up Productivity: The Effects of Electrification on US Manufacturing," *NBER Working Paper*, 2020, (w28076). [5]

Fontagné, Lionel, Houssein Guimbard, and Gianluca Orefice, "Tariff-based Product-level Trade Elasticities," *Journal of International Economics*, 2022, *137*, 103593. [22, 25]

Fröling, Maria, "Energy Use, Population and Growth, 1800–1970," *Journal of Population Economics*, 2011, *24* (3), 1133–1163. [5]

Golosov, Mikhail, John Hassler, Per Krusell, and Aleh Tsyvinski, "Optimal Taxes on Fossil Fuel in General Equilibrium," *Econometrica*, 2014, *82* (1), 41–88. [4]

Gorman, Will, Cristina Crespo Montañés, Andrew Mills, James Hyungkwan Kim, Dev Millstein, and Ryan Wiser, "Are Coupled Renewable-Battery Power Plants More Valuable than Independently Sited Installations?," *Energy Economics*, 2022, *107*, 105832. [12]

Gutman, Richard, PP Marchenko, and RD Dunlop, "Analytical Development of Loadability Characteristics for EHV and UHV Transmission Lines," *IEEE Transactions on Power Apparatus and Systems*, 1979, (2), 606–617. [A13]

Hanson, Gordon H, "Local Labor Market Impacts of the Energy Transition: Prospects and Policies," Technical Report, National Bureau of Economic Research 2023. [39]

Head, Keith and Thierry Mayer, "Gravity Equations: Workhorse, Toolkit, and Cookbook," in "Handbook of international economics," Vol. 4, Elsevier, 2014, pp. 131–195. [22]

Hodgson, Charles, *Information Externalities, Free riding, and Optimal Exploration in the UK Oil Industry*, SIEPR, Stanford Institute for Economic Policy Research, 2019. [4]

Hotelling, Harold, "The Economics of Exhaustible Resources," *Journal of political Economy*, 1931, *39* (2), 137–175. [16]

Jordan, Dirk C and Sarah R Kurtz, "Photovoltaic Degradation Rates An Analytical Review," *Progress in Photovoltaics: Research and Applications*, 2013, *21* (1), 12–29. [24]

Kleinman, Benny, Ernest Liu, and Stephen J Redding, "Dynamic Spatial General Equilibrium," *Econometrica*, 2023, *91* (2), 385–424. [16]

Kline, Patrick and Enrico Moretti, "Local Economic Development, Agglomeration Economies and the Big Push: 100 Years of Evidence from the Tennessee Valley Authority," *Quarterly Journal of Economics*, 2014, *129*, 275–331. [5]

Kortum, Samuel S and David A Weisbach, "Optimal Unilateral Carbon Policy," 2021. [4]

Krusell, Per and Anthony A Smith Jr, "Climate Change Around the World," Technical Report, National Bureau of Economic Research 2022. [4]

Kypreos, Socrates and Olivier Bahn, "A MERGE Model with Endogenous Technological Progress," *Environmental Modeling & Assessment*, 2003, *8*, 249–259. [5]

Lamont, Alan D, "Assessing the Long-term System Value of Intermittent Electric Generation Technologies," *Energy Economics*, 2008, *30* (3), 1208–1231. [26]

Lazard, L, "Lazard's Levelized Cost of Energy Analysis," Technical Report 2019. [16]

McDonald, Alan and Leo Schrattenholzer, "Learning Rates for Energy Technologies," *Energy policy*, 2001, *29* (4), 255–261. [1]

Mehigan, L, Dlzar Al Kez, Seán Collins, Aoife Foley, Brian Ó'Gallachóir, and Paul Deane, "Renewables in the European Power System and the Impact on System Rotational Inertia," *Energy*, 2020, *203*, 117776. [12]

Moneke, Niclas, "Can Big push Infrastructure Unlock Development? Evidence from Ethiopia," *STEG Theme*, 2020, *3*, 14–15. [5]

Moretti, Enrico, "Real Wage Inequality," *American Economic Journal: Applied Economics*, 2013, *5* (1), 65–103. [5]

Mulder, FM, "Implications of Diurnal and Seasonal Variations in Renewable Energy Generation for Large Scale Energy Storage," *Journal of Renewable and Sustainable Energy*, 2014, *6* (3), 033105. [11]

Newbery, David, "Evaluating the Case for Supporting Renewable Electricity," *Energy Policy*, 2018, *120*, 684–696. [1]

Nordhaus, William D, "The Perils of the Learning Model for Modeling Endogenous Technological Change," *The Energy Journal*, 2014, *35* (1). [24]

_ , **Hendrik Houthakker, and Robert Solow**, "The Allocation of Energy Resources," *Brookings Papers on Economic Activity*, 1973, *1973* (3), 529–576. [5]

Nykvist, Björn and Måns Nilsson, "Rapidly Falling Costs of Battery Packs for Electric Vehicles," *Nature Climate Change*, 2015, *5* (4), 329–332. [12]

Perlin, John, *From Space to Earth: the Story of Solar Electricity*, Earthscan, 1999. [1]

Redding, Stephen J and Esteban Rossi-Hansberg, "Quantitative spatial economics," *Annual Review of Economics*, 2017, *9*, 21–58. [4, 22]

Roser, Max, "Why Did Renewables Become So Cheap So Fast?," *World in Data*, 2020. [1]

Rubin, Edward S, Inês ML Azevedo, Paulina Jaramillo, and Sonia Yeh, "A Review of Learning Rates for Electricity Supply Technologies," *Energy Policy*, 2015, *86*, 198–218. [1]

Rud, Juan Pablo, "Electricity Provision and Industrial Development: Evidence from India," *Journal of Development Economics*, 2012, *97* (2), 352–367. [5]

Sahraei-Ardakani, Mostafa, Seth Blumsack, and Andrew Kleit, "Estimating Zonal Electricity Supply Curves in Transmission-constrained Electricity Markets," *Energy*, 2015, *80*, 10–19. [23]

SETO, "2030 Solar Cost Targets," 2021. [28]

Shaner, Matthew R, Steven J Davis, Nathan S Lewis, and Ken Caldeira, "Geophysical Constraints on the Reliability of Solar and Wind Power in the United States," *Energy & Environmental Science*, 2018, *11* (4), 914–925. [12, 31]

Stern, David I, "Interfuel Substitution: a Meta-analysis," *Journal of Economic Surveys*, 2012, *26* (2), 307–331. [23, 25]

_ , "Energy and Economic Growth," in "Routledge Handbook of Energy Economics," Routledge, 2019, pp. 28–46. [4]

Tahvonen, Olli and Seppo Salo, "Economic Erowth and Transitions Between Renewable and Nonrenewable Energy Resources," *European Economic Review*, 2001, *45* (8), 1379–1398. [5]

Tangeras, Thomas P and Frank A Wolak, "The Competitive Effects of Linking Electricity Markets Across Space," Technical Report, IFN Working Paper 2021. [5, 14]

Thissen, Mark, Maureen Lankhuizen, Frank van Oort, Bart Los, and Dario Diodato, "EUREGIO: The Construction of a Global IO DATABASE with Regional Detail for Europe for 2000–2010," 2018. [21]

Thompson, Peter, "Learning by doing," *Handbook of the Economics of Innovation*, 2010, *1*, 429–476. [24]

Tong, Dan, David J Farnham, Lei Duan, Qiang Zhang, Nathan S Lewis, Ken Caldeira, and Steven J Davis, "Geophysical Constraints on the Reliability of Solar and Wind Power Worldwide," *Nature communications*, 2021, *12* (1), 6146. [12, 31, A13]

U.S. Energy Information Administration, "Annual Energy Outlook 2022," March 2022. [24]

Walsh, Conor, "Local Growth Policy and Dynamic Misallocation," 2021. [4]

Welsby, Dan, James Price, Steve Pye, and Paul Ekins, "Unextractable Fossil Fuels in a 1.5 C World," *Nature*, 2021, *597* (7875), 230–234. [20, 25, A9]

Wiser, Ryan H and Mark Bolinger, "Benchmarking Anticipated Wind Project Lifetimes: Results from a Survey of US Wind Industry Professionals," Technical Report, Lawrence Berkeley National Lab.(LBNL), Berkeley, CA (United States) 2019. [24]

Wolak, Frank A, "Financing the Energy Transition in a Low-Cost Intermittent Renewables Environment," 2021. [5]

Woo, Chi-Keung, Jack Moore, Brendan Schneiderman, Tony Ho, Arne Olson, Lakshmi Alagappan, Kiran Chawla, Nate Toyama, and Jay Zarnikau, "Merit-order Effects of Renewable Energy and Price Divergence in California Day-ahead and Real-time Electricity Markets," *Energy Policy*, 2016, *92*, 299–312. [8]

Ziegler, Micah S and Jessika E Trancik, "Data series for Lithium-ion Battery Technologies," *https://doi.org/10.7910/DVN/9FEJ7C,*, 2021. [33, A7]

_ **and** _ , "Re-examining Rates of Lithium-ion Battery Technology Improvement and Cost Decline," *Energy & Environmental Science*, 2021, *14* (4), 1635–1651. [33, A7]

A1 Additional Figures and Tables

In this section we provide additional figures to the paper. Figure A2 plots the raw power station data and transmission line data over the globe. Figure A3 plots the representation of this data for Europe and China which we use in the model. Figure A6 plots the aggregate learning rates for solar and wind capital in the data. Figure A8 plots Locational Marginal Prices for the US in 2020, as well as the model generated prices in each one of the US regions in 2020.

Figure A1: Aggregate Capacity Additions

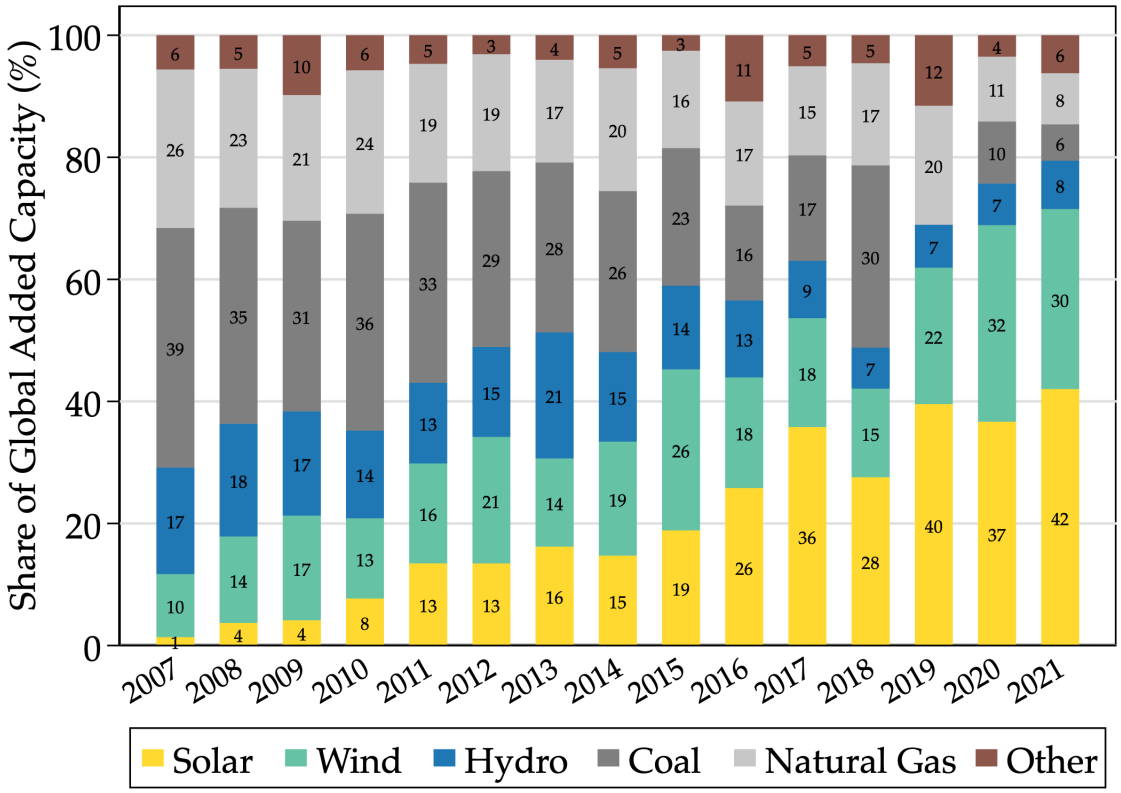

Notes: This figure plots the share of total new generating capacity across the globe by type. Data is from the International Renewable Energy Agency.

Figure A2: Global Power Capital

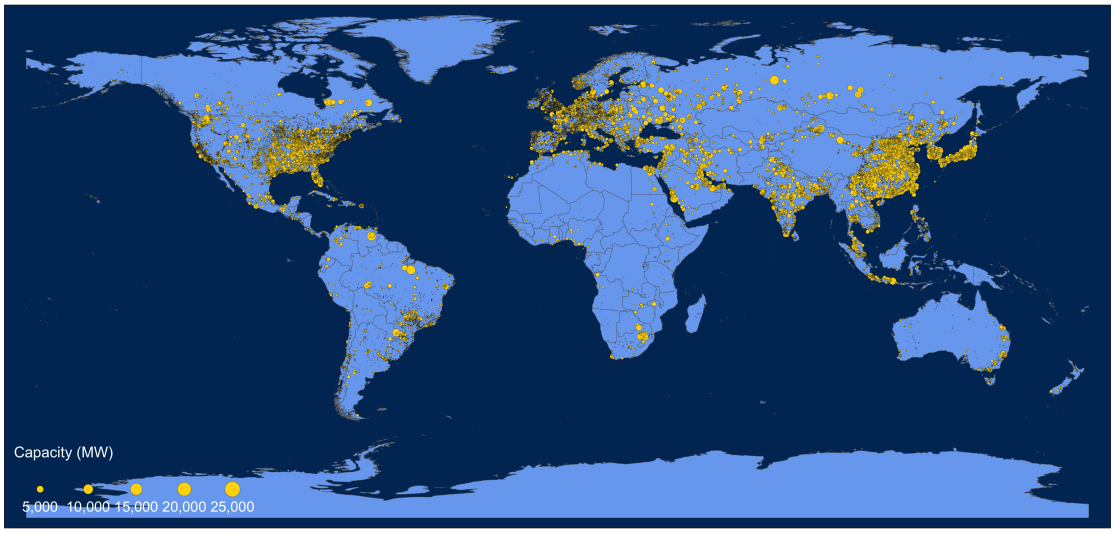

Notes: This figure shows installed power capital in MW using data from the World Resources Institute.

Figure A3: Network Representations for Other Major Regions

(a) China

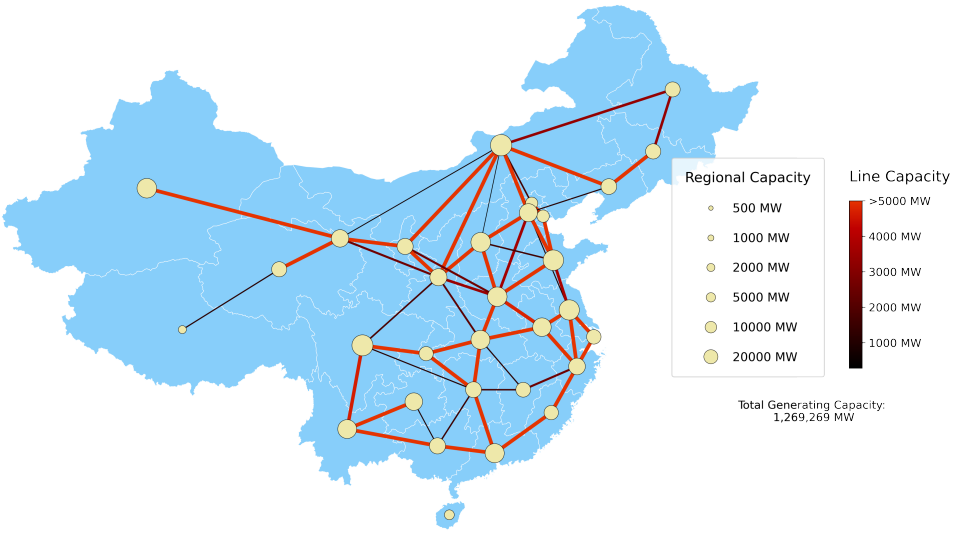

(b) Europe

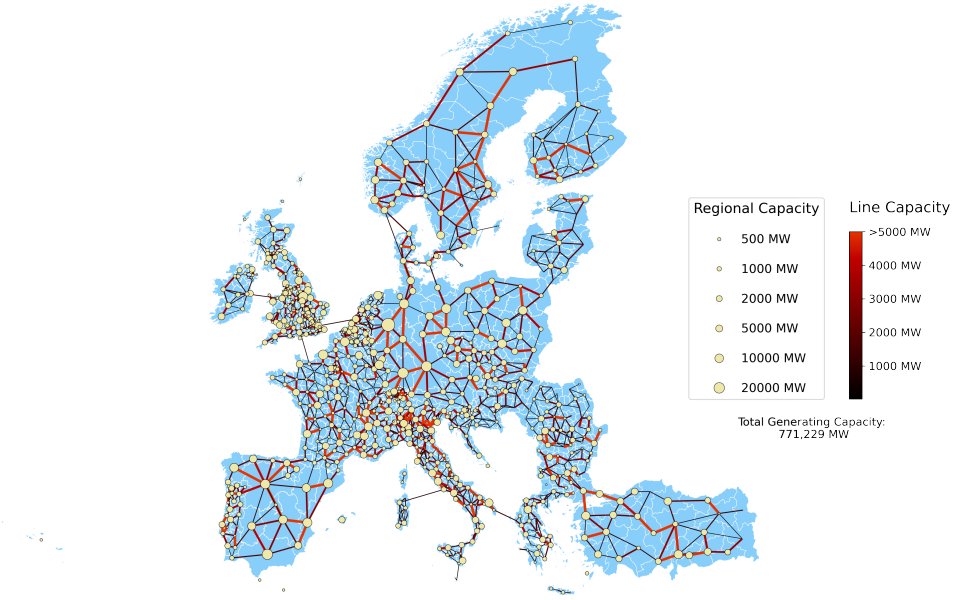

Notes: This figure shows a representation of the electrical grid between regions of China (Panel (a)) and Europe (Panel (b)) using data from Openstreetmap (transmission lines) and the World Resources Institute Database (power capital). Circle size is proportional to region generating capacity in MW. Line thickness is proportional to the number of transmission lines between regions

Figure A4: Network Representations for Other Major Regions (2)

(a) India

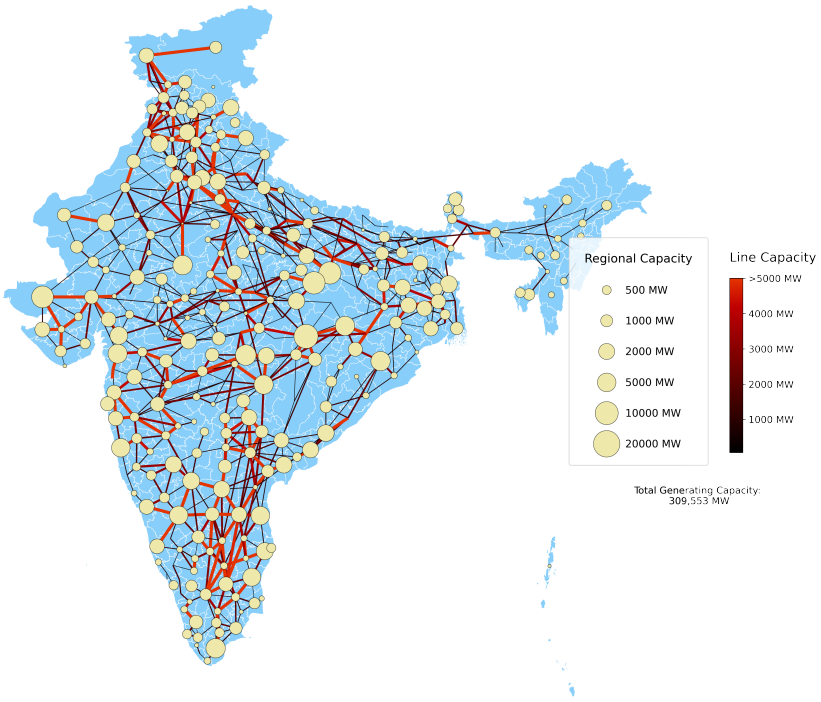

(b) Brazil

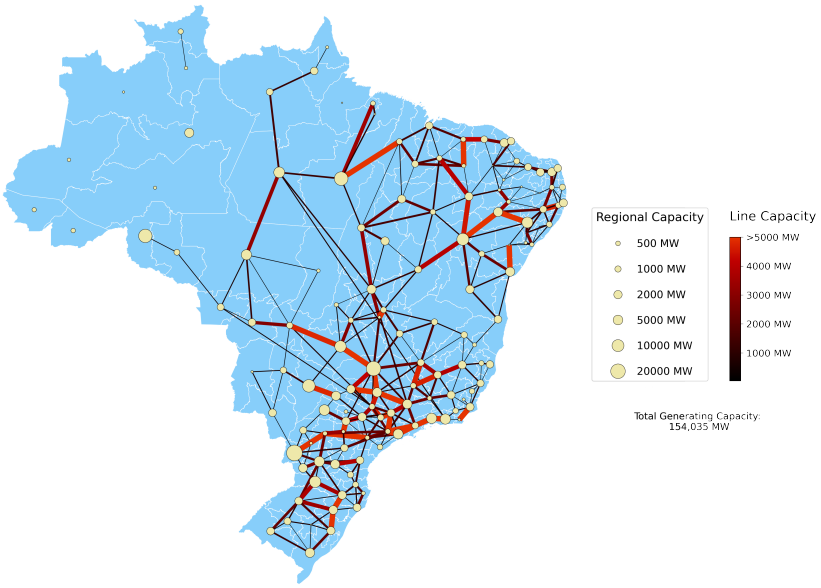

Notes: This figure shows a representation of the electrical grid between regions of India (Panel (a)) and Brazil (Panel (b)) using data from Open Street Map (transmission lines) and the World Resources Institute Database (power capital). Circle size is proportional to region generating capacity in MW. Line thickness is proportional to the number of transmission lines between regions

Figure A5: World Regions

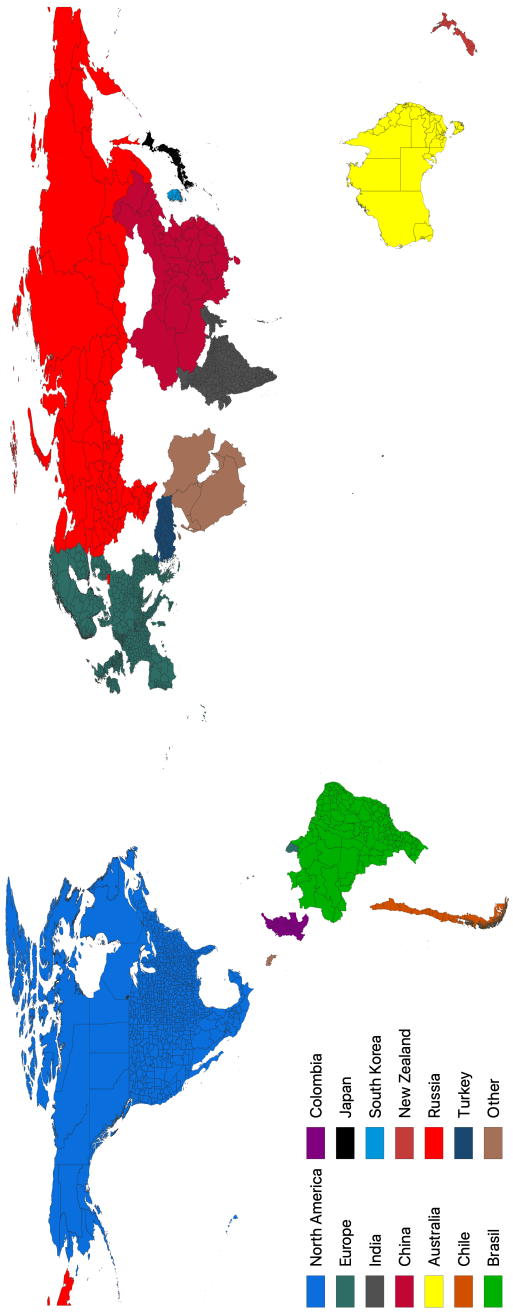

Notes: This figure shows the selected regions for the world, with colors indicating the zones we treat as integrated grids.

Figure A6: Aggregate Learning Rates for Power Technologies

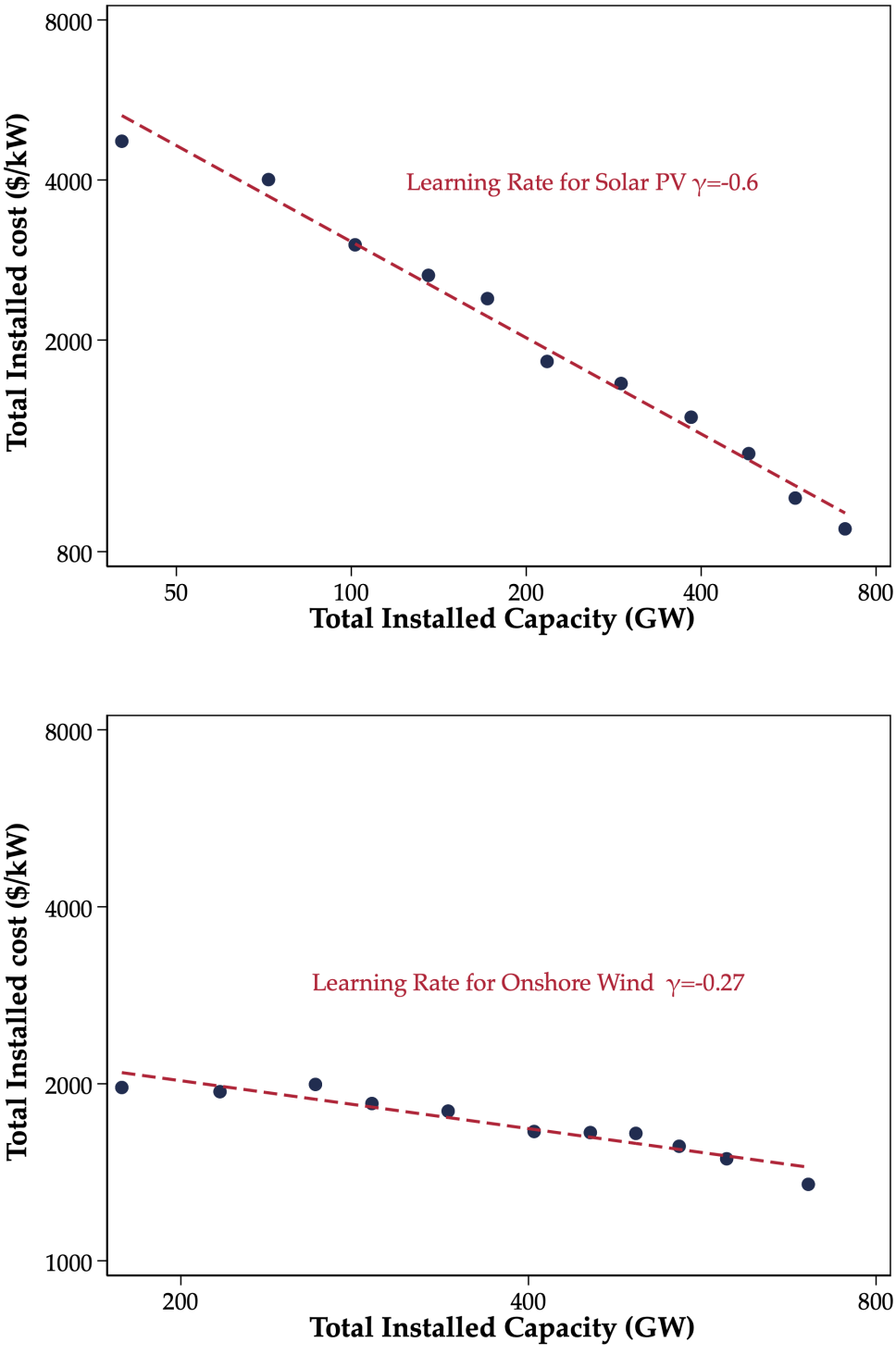

Notes: This figure plots the total installed cost of capacity from a new solar and wind energy project against world installed capacity. Data is from the International Renewable Energy Agency. Values are in constant 2019 dollars. Data is from 2009-2019.

Figure A7: Aggregate Learning Rates for Lithium-Ion Batteries

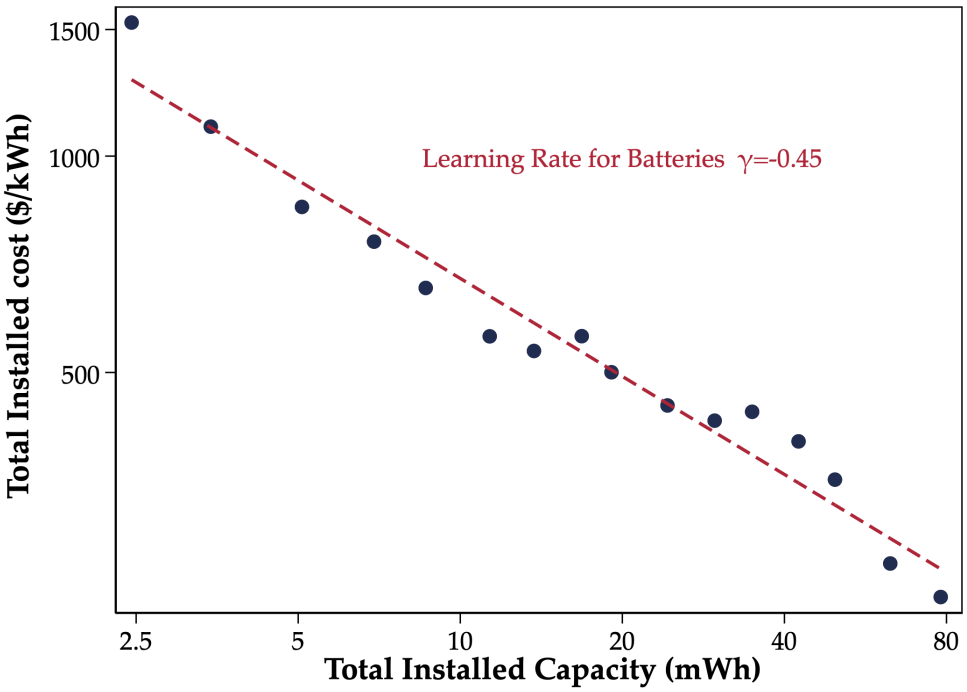

Notes: This figure plots the total installed cost against world installed capacity for lithium-ion batteries. Values are in constant 2018 dollars. Data is from 2000-2016 using Ziegler and Trancik (2021b), available from Ziegler and Trancik (2021a).

Figure A8: Spatial Electricity Prices

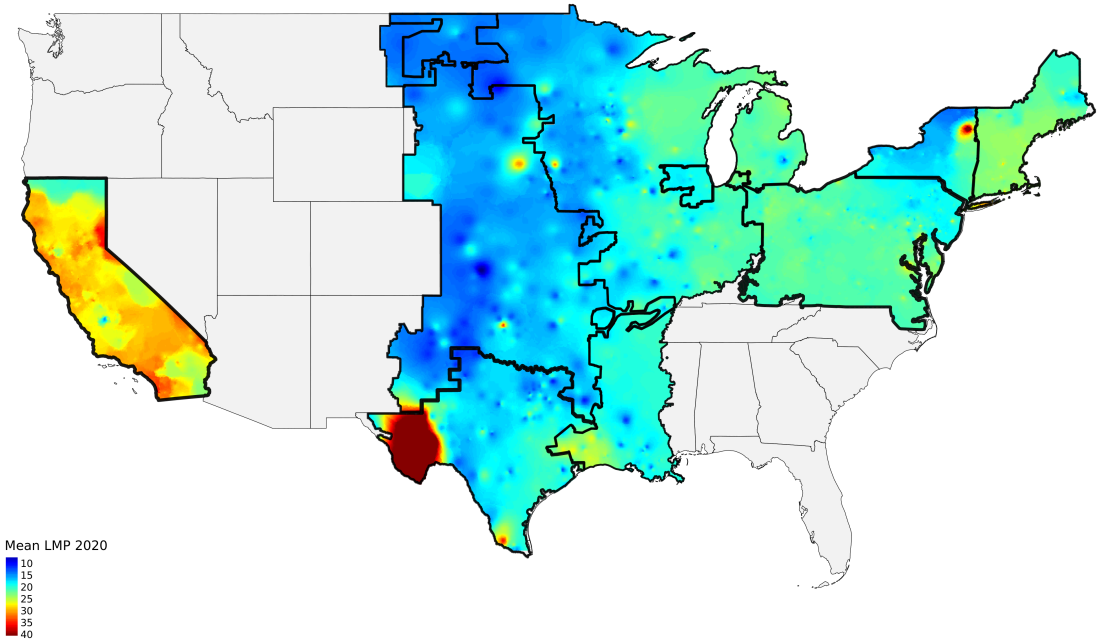

(a) Data

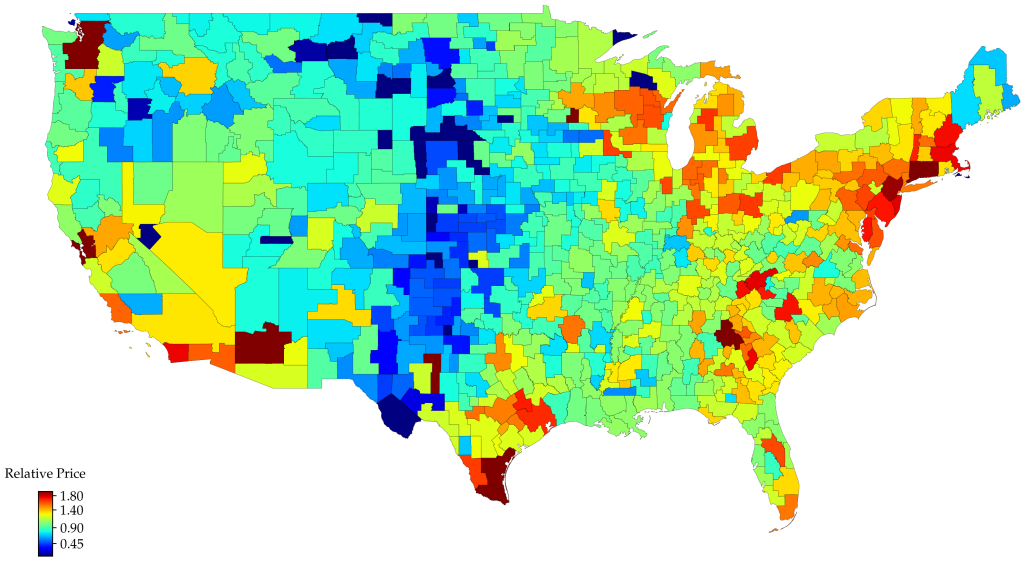

(b) Model

Notes: The top panel of this figures show locational marginal prices from 9 RTO/ISOs in the continental US. Data are averagedx at each pricing node for 2020, and then smoothed over space. The bottom panel shows the model predictions for prices in 2020 for all US commuting zones.

Figure A9: World Fossil Resources

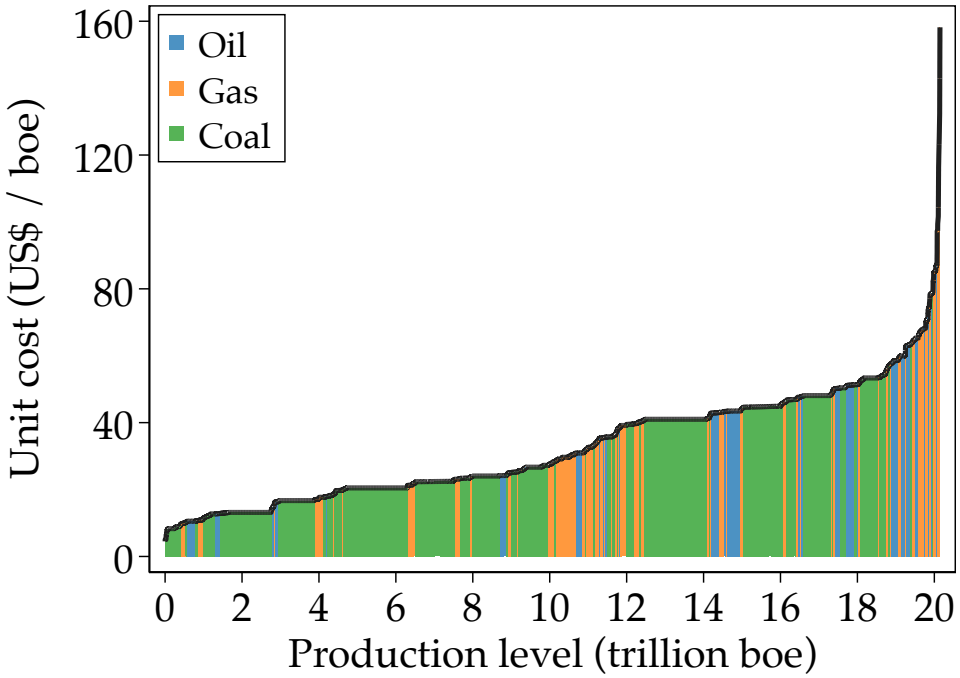

Notes: This figure shows the fossil fuel resources of the globe ordered by current (2021) extraction cost for three types of fuel: coal, oil and natural gas. The source data is from Welsby et al. (2021).

Figure A10: Long-Run Welfare Changes

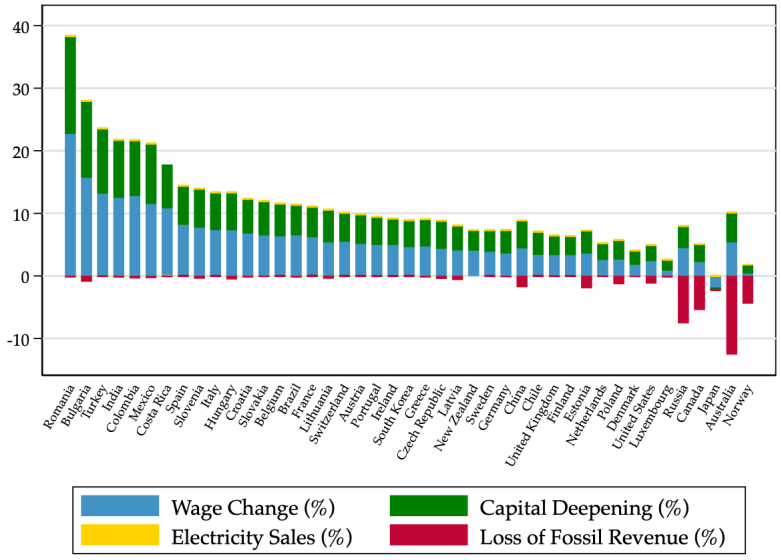

Notes: This Figure shows the welfare changes in the long-run steady state at the country level. Welfare changes across regions are aggregated to the country level via an employment weighted average. The decomposition of these changes is computed according to equation (25).

Figure A11: Curtailment with 0 and 4 hours of Battery Storage

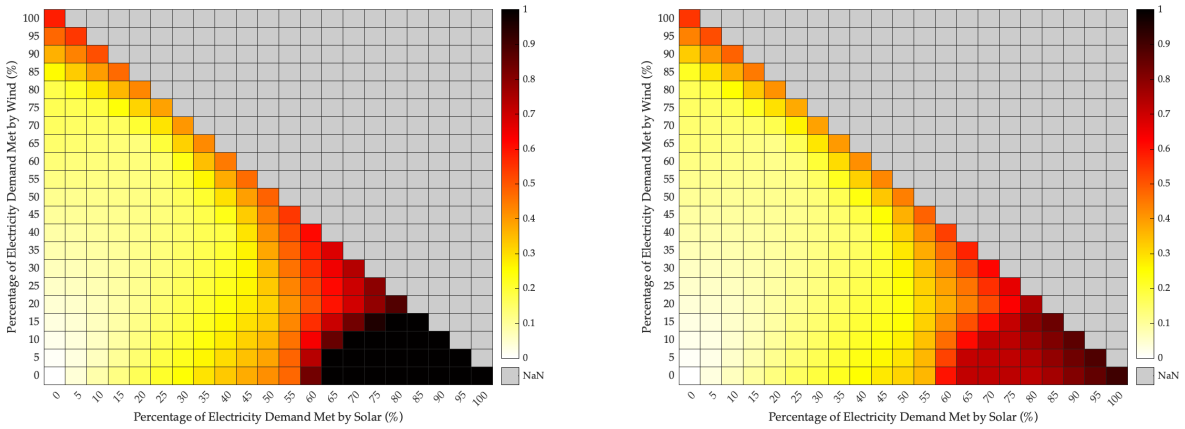

Notes: The left panel shows curtailment as a function of wind and solar penetration in the US under no hours of battery storage, and the right the same figure under 4 hours of battery storage.

Figure A12: Worst Case Battery Storage Requirements for Curtailment <50%

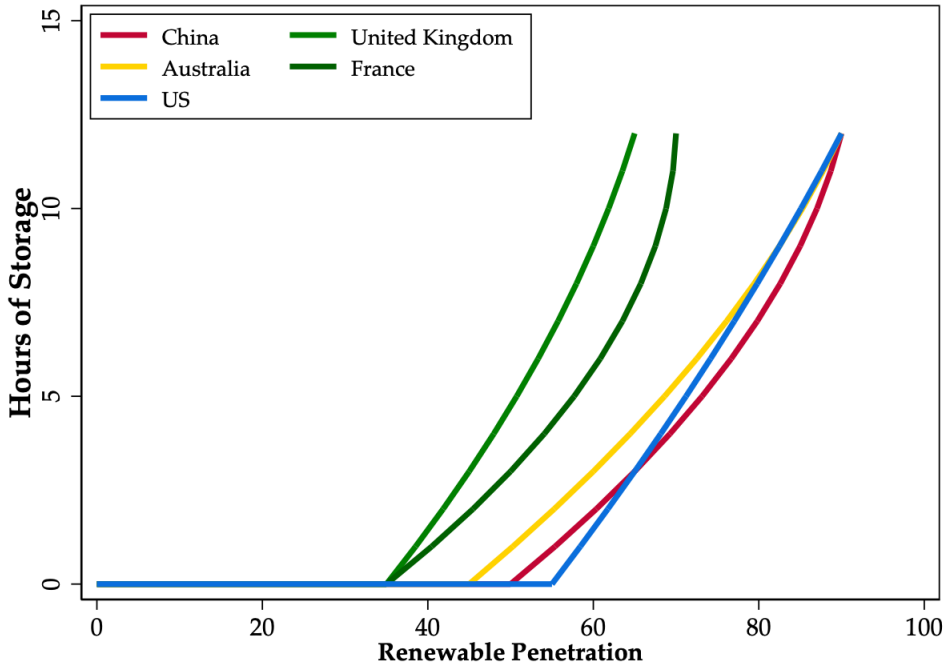

Notes: This figure shows the required amount of battery storage in the worst case scenario of renewable penetration to keep curtailment under 50%, for selected countries.

Figure A13: Renewable Shares in the US with 4 hours of Storage Requirements

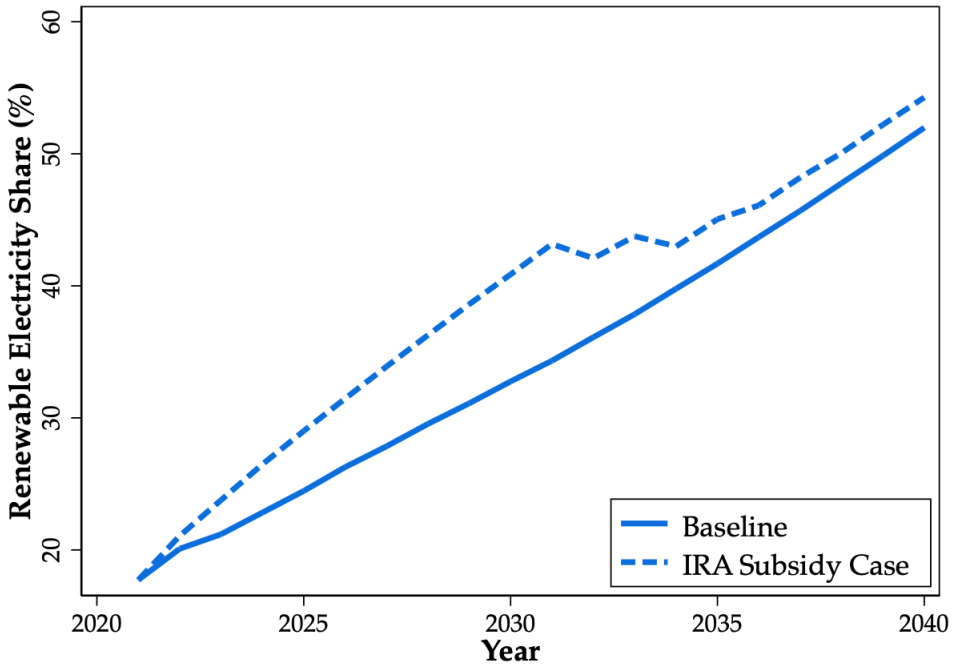

Notes: This figure shows the renewable share of electricity in the US when requiring 4 hours of storage per unit of capital, under both the IRA subsidy and without.

A2 Data Construction for the Electricity Grid

In this section we provide details about the construction of data used in the paper. The data consists of two primary components: asset data and grid data. Greater detail is given in the Supplementary Material. Details about the other regional datasets used throughout the paper are also provided in the Supplementary Material.

A2.1 Power Assets

To generate the asset data we use the Global Power Plant (GPP) database, which consists of over 35,000 power plants in 167 countries, each with a name, primary fuel type, geolocation, and power capacity information. We cross-reference the data with official sources from numerous countries to ensure accuracy.[25]

A2.2 Electrical Grid

We use Open Street Map (OSM) data and a Java tool called Osmosis to filter out all non-power-grid data. After filtering we perform further cleaning on the extracted data. We use the power stations and plants in the OSM data extensively in the cleaning process to determine the start and end points of transmission line segments but use the asset data from GPP as this dataset is far richer for assets. The following is a high-level summary of the operations performed by our algorithm, see the Supplementary Material for more details.

At any given location, there may be multiple polygons representing different buildings or components within the same "station". We use the term "station" as a catch-all term to describe plants, stations, substations and transformers. As such, we cluster stations within 500 meters of each other.[26] After clustering the stations, we replace line endpoints with the relevant station centroids, either stations intersecting or within 500 meters of the of line, at each step. Spot checks on Google Earth confirm that many lines that actually connect to nearby stations in reality are not captured by an intersection in the OSM data; instead the lines end outside of the polygon. Incorporating nearby stations addresses this problem. After we complete the line endpoint replacement, lines which are intersected by one or more stations are split. As a result a unique line is defined as one that connects at most two stations. This is also done for stations that are within 500 meters of lines by taking the closest point on the line to the nearby station, buffering it to account for tolerance issues, and subtracting that buffered object from the line. Each line is given a new unique ID number after splitting.

We merge lines together when they have separate IDs and are connected, or are within 500 meters of each other with no station in between. For T-intersections, we take two approaches. A T-intersection is defined as an intersection between two lines A and B where A intersects (or lies within a 500 meter radius of) Line B but not at line B's endpoint. In cases where the relationship is symmetric

[25] Our version of the data was downloaded on November 30, 2020.

[26] This involves grouping stations within 500 meters of one another and taking the convex hull of each group as our final station.

between A and B, we combine the lines into a single line. When the T-intersection is not symmetric (the more common case), the top of the T is split by the bottom, and an artificial station called an "auxiliary" station is constructed at that point to keep track of the intersection. Next, lines which do not intersect any other lines at endpoints are removed and all lines are straightened between their endpoints. Finally, lines which do not intersect any stations or other lines are dropped.

We impute line capacity using the St Clair curve (see Gutman et al. (1979)) and information on line voltage and distance.

The post-algorithm grid data and the GPP asset data are both granular because each observation is at the line or station level. As such, we aggregate assets and grid lines using the same geographical borders as for our employment.

A3 Data Construction for Curtailment

In this section we discuss the details of the construction of curtailment factors for different countries. The construction entails two steps.

In the first step, we use Tong et al. (2021) to extract data from Figure 2 of their paper, which contain the following variables: generation capacity as a function of the overall demand (e.g. 1x generation is capacity potential as much as demand), storage level under no storage, 3 hours of storage, 12 hour storage and for the available wind and solar mix. We use a color picker, Digital Color Meter in Macintosh, to extract the color of a particular value in the figure along with a program that extracts the correct scales of the color from the figure. The output for this is the reliability of a renewable resource measured by the authors, i.e. the percentage of energy demand met by the resource.

Using these data as input we then generate the curtailment matrix for each generation capacity. Finally, we interpolate the missing points using linear interpolation, and generate heatmaps for each country for no storage, 2, 4, and 8 hours of storage.

A4 Electrical Line Losses

In this section we derive network losses as a function of power injections and withdrawals in the network. This discussion follows Bohn et al. (1984), where we have provided additional detail for clarity. We consider lines with resistance R_k and inductance X_k. The impedance magnitude is $z_k = (X_k^2 + R_k^2)^{\frac{1}{2}}$, which is sufficient to compute the losses, and we call

$$\Omega_k = z_k^{-1} \tag{A1}$$

the admittance of a line. Let S denote the sending end of the line and R the receiving. Ohm's law for AC circuits gives that the current flowing out of S is equal to

$$I_S = \frac{V_S - V_R}{B_k},$$

where I_S is the current at the sending end of the line, $V_S - V_R$ is the voltage drop across the line k, and B_k is the impedance of the line. These are complex-valued variables, and have an associated magnitude and angle, such that

$$I_S = \frac{|V_S|e^{j\delta_S} - |V_R|e^{j\delta_R}}{|z_k|e^{jb}},$$

where δ_S and δ_R are the voltage angles in S and R and b is the angle shift induced by the line itself. Following the notation of the electrical engineering literature, $j = \sqrt{-1}$. Define $\Delta \equiv \delta_S - \delta_R$. The same expression holds for I_R. Apparent power is defined as

$$T_S = Z_S + jQ_S = V_S I_S^*;$$
$$T_R = Z_R + jQ_R = V_R I_R^*,$$

where Z is real power (the component of power that can do useful work) and Q is reactive power. This can be written in polar form as

$$T_S = \Omega_k |V_S| \left(|V_S|e^{j(b)} - |V_R|e^{j(b-(\delta_R-\delta_S))} \right);$$
$$T_R = \Omega_k |V_R| \left(|V_S|e^{j(b-(\delta_S-\delta_R))} - |V_R|e^{jb} \right).$$

Now assuming that voltages are constant and unitized everywhere ($|V_S| = |V_k| = 1$), we can write real power flows out of S and into R as

$$Z_S = \Omega_k(cos(b_k) - cos(b_k + \Delta_k));$$

$$Z_R = \Omega_k(cos(b_k) - cos(b_k - \Delta_k)).$$

Note that with power flowing from S to R, we have $P_S > 0 > P_R$. Total real power losses on the line are

$$\lambda_k = Z_S + Z_R = \Omega_k 2cos(b_k) - \Omega_k(cos(b_k - \Delta_k) + cos(b_k + \Delta_k))$$

which can be written

$$\lambda_k = \Omega_k 2cos(b_k) - \Omega_k 2cos(b_k)cos(\Delta_k) =$$

$$= \Omega_k 2cosb_k(1 - cos(\Delta_k)) \approx \Omega_k 2\left(cos(b_k)\right)\left(\frac{\Delta_k^2}{2}\right) = R_k\Omega_k^2\Delta_k^2, \tag{A2}$$

where in the second line we have used a second-order approximation to $1 - cos(\Delta) \approx \Delta^2/2$, assuming that Δ_k is small, and that $b_k = cos^{-1}(R_k/z_k)$ and the definition in (A1). Note also that

$$Z_k = \Omega_k(cos(b) - cos(b + \Delta)) = \Omega_k 2sin\left(\frac{2b + \Delta_k}{2}\right) sin\left(\frac{\Delta_k}{2}\right) \approx \Omega_k^2 X_k \Delta_k,$$

where we have taken a second order expansion as Δ_k becomes small. Now assuming that $R_k << X_k$, we have $\Omega_k^{-1} = z_k \approx X_k$. So we can write

$$Z_S = \Omega_k \Delta_k, \tag{A3}$$

and using (A2) we finally arrive at

$$\lambda_k = R_k(Z_S)^2. \tag{A4}$$

As above, let $\bar{\boldsymbol{A}}$ be the *bus-branch incidence matrix* of dimension $K \times (N-1)$. Each row consists of a 1, a -1 and zeros. The "direction" of a power-line is arbitrary (i.e. suppose line k has a 1 for node m and -1 for node n in the matrix $\bar{\boldsymbol{A}}$. Then a positive value for Z_k indicates net real power flow from m to n, while a negative value will show power flowing in the other direction). Power injections $P_j = Y_j^{\mathcal{E}} - D_j$ must satisfy

$$\boldsymbol{P} = \bar{\boldsymbol{A}}'\boldsymbol{Z}, \tag{A5}$$

such that power injected equals the sum of flows out of the bus. The J^{th} node is called the "swing bus", and power flows there are determined by the energy balance constraint, which can be written

$$\boldsymbol{e}'\boldsymbol{P} + P_J - \lambda = 0,$$

where $\boldsymbol{e}$ is a $(J-1)$ vector of ones, and $\lambda = \sum_k \lambda_k$ is total system losses. Now, the incidence matrix $\bar{\boldsymbol{A}}$ allows us to write all the voltage differences $\boldsymbol{\Delta}$ on each line as

$$\underset{K\times N-1}{\boldsymbol{\Delta}} = \bar{\boldsymbol{A}}\,\delta,$$

where δ is a $N-1$ vector of voltage phase differences on each node from the swing bus. Now using equation (A3), we can write the $K \times 1$ vector of power flows $\boldsymbol{Z}$ as

$$\boldsymbol{Z} = \bar{\boldsymbol{\Omega}}\boldsymbol{\Delta},$$

where $\bar{\Omega}$ is a $K \times K$ diagonal matrix of line admittances with $\Omega_k = (R_k^2 + X_k^2)^{-\frac{1}{2}}$ on the diagonal and 0 on the off-diagonal elements. Combine this with (A5) to get

$$\boldsymbol{P} = \bar{\boldsymbol{A}}'\bar{\boldsymbol{\Omega}}\bar{\boldsymbol{A}}\delta,$$

and use this to get the voltage angles

$$\delta = (\underset{N-1\times KK\times KK\times N-1}{\bar{\boldsymbol{A}}'\,\bar{\boldsymbol{\Omega}}\,\bar{\boldsymbol{A}}})^{-1}\underset{N-1\times 1}{\boldsymbol{P}}$$

in terms of properties of the electricity network. Finally, the flows on each line are

$$\boldsymbol{Z} = \bar{\boldsymbol{\Omega}}\bar{\boldsymbol{A}}(\bar{\boldsymbol{A}}'\bar{\boldsymbol{\Omega}}\bar{\boldsymbol{A}})^{-1}\boldsymbol{P}. \tag{A6}$$

Lastly, let $\bar{\boldsymbol{R}}$ be a diagonal matrix with R_k on the diagonal. Using (A4), we can write

$$\lambda = \boldsymbol{Z}'\bar{\boldsymbol{R}}\boldsymbol{Z}. \tag{A7}$$

A5 Proofs and Additional Results

A5.1 Lemma 1

Proof. With constant resistance-inductance ratio across all lines, we have $\bar{\boldsymbol{R}} = \alpha\bar{\boldsymbol{\Omega}}^{-1}$ for some positive α. Replace $\boldsymbol{Z}$ in (A7) using (A6) and obtain

$$\begin{aligned}\lambda &= \left(\bar{\boldsymbol{\Omega}}\bar{\boldsymbol{A}}(\bar{\boldsymbol{A}}'\bar{\boldsymbol{\Omega}}\bar{\boldsymbol{A}})^{-1}\boldsymbol{P}\right)' \alpha\bar{\boldsymbol{\Omega}}^{-1}\bar{\boldsymbol{\Omega}}\bar{\boldsymbol{A}}(\bar{\boldsymbol{A}}'\bar{\boldsymbol{\Omega}}\bar{\boldsymbol{A}})^{-1}\boldsymbol{P} \\ &= \alpha\boldsymbol{P}'(\bar{\boldsymbol{A}}'\bar{\boldsymbol{\Omega}}\bar{\boldsymbol{A}})^{-1}\bar{\boldsymbol{A}}'\bar{\boldsymbol{\Omega}}\bar{\boldsymbol{A}}(\bar{\boldsymbol{A}}'\bar{\boldsymbol{\Omega}}\bar{\boldsymbol{A}})^{-1}\boldsymbol{P} \\ &= \alpha\boldsymbol{P}'(\bar{\boldsymbol{A}}'\bar{\boldsymbol{\Omega}}\bar{\boldsymbol{A}})^{-1}\boldsymbol{P}\end{aligned}$$

Define

$$\bar{\boldsymbol{B}} \equiv \alpha(\bar{\boldsymbol{A}}'\bar{\boldsymbol{\Omega}}\bar{\boldsymbol{A}})^{-1} = (\bar{\boldsymbol{A}}'\bar{\boldsymbol{R}}^{-\mathbf{1}}\bar{\boldsymbol{A}})^{-1}$$

Now note we can write

$$\bar{\boldsymbol{A}}'\bar{\boldsymbol{R}}^{-\mathbf{1}}\bar{\boldsymbol{A}} = \left(\bar{\boldsymbol{R}}^{-\frac{\mathbf{1}}{\mathbf{2}}}\bar{\boldsymbol{A}}\right)' \bar{\boldsymbol{R}}^{-\frac{\mathbf{1}}{\mathbf{2}}}\bar{\boldsymbol{A}}$$

since $\bar{\boldsymbol{R}}$ is diagonal. Then since $\bar{\boldsymbol{A}}$ has linearly independent columns by inspection, $\bar{\boldsymbol{R}}^{-\frac{\mathbf{1}}{\mathbf{2}}}\bar{\boldsymbol{A}}$ has linearly independent columns. Recall that a matrix is positive semidefinite if and only if it can be written as $\bar{\boldsymbol{X}} = \bar{\boldsymbol{Y}}'\bar{\boldsymbol{Y}}$ for some possibly rectangular matrix $\bar{\boldsymbol{Y}}$ with independent columns. Now $rank(\bar{\boldsymbol{R}}^{-\frac{\mathbf{1}}{\mathbf{2}}}\bar{\boldsymbol{A}}) = J - 1$. Recall that for any decomposition $\bar{\boldsymbol{X}} = \bar{\boldsymbol{Y}}'\bar{\boldsymbol{Y}}$, $rank(\bar{\boldsymbol{X}}) = rank(\bar{\boldsymbol{Y}})$. So $\bar{\boldsymbol{A}}'\bar{\boldsymbol{R}}^{-\mathbf{1}}\bar{\boldsymbol{A}}$ is invertible, and positive definite, and so is its inverse. □

A5.2 Proposition 1

Proof. Begin by with the problem of the planner who picks quantities $Y_j^{\mathcal{E}}$ and D_j to maximize the sum of consumer and producer surplus. Choose a node b as the reference "swing bus". We can rewrite the planner's problem by substituting in the power balance constraint into the objective function to get

$$\max_{\{P_j\},\{D_{js}\}} \sum_j \sum_s p_{js}q_{js}(D_{js}) - \sum_{j\neq b} M_j(P_j + D_j) - M_b\left(\boldsymbol{P}'\bar{\boldsymbol{B}}\boldsymbol{P} + D_b - \sum_{j\neq b} P_j\right) \tag{A8}$$

subject to

$$D_j = \sum_s D_{js}$$

$$0 \leq P_j + D_j \leq \bar{Y}_j^{max} \tag{A9}$$

$$|\bar{\boldsymbol{\Omega}}\bar{\boldsymbol{A}}(\bar{\boldsymbol{A}}'\bar{\boldsymbol{\Omega}}\bar{\boldsymbol{A}})^{-1}\boldsymbol{P}| \leq \boldsymbol{Z}^{max} \tag{A10}$$

Note that $G_j(\boldsymbol{P},\boldsymbol{D}) = P_j + D_j$ is convex, and $H(\boldsymbol{P},\boldsymbol{D}) = \boldsymbol{P}'\bar{\boldsymbol{B}}\boldsymbol{P} + D_b - \sum_{j\neq b} P_j$ is convex by the positive definiteness of $\bar{\boldsymbol{B}}$ (see Lemma 1). . Then since M_j and M_b are non-decreasing convex functions, $\sum_{j\neq b} M_j(P_j + D_j) + M_b(\boldsymbol{P}'\bar{\boldsymbol{B}}\boldsymbol{P} - \sum_{j\neq b} P_j + D_b)$ is convex. Hence the planner's objective function maximizes a strictly concave function over a convex set defined by the linear inequality

constraints in (A9) and (A10).

Then all that remains to show is that this solution can be implemented by choosing prices appropriately. The FOC's of the original planning problem are

$$p_{js}q'_{js}(D_{js}) - \sum_k \eta_k \frac{\partial Z_k}{\partial D_{js}} - \mu\left(1 + \frac{\partial \lambda}{\partial D_{js}}\right) = 0$$

$$-M'_j(Y_j^{\mathcal{E}}) - \mu_j - \sum_k \eta_k \frac{\partial Z_k}{\partial Y_j} - \mu\left(-1 + \frac{\partial \lambda}{\partial Y_j}\right) = 0$$

where η_k are the Lagrange multipliers on additional line capacity on line k, μ is the multiplier on total system generation and μ_j is the multiplier on extra generating capacity at j. Note that by the definition of $\boldsymbol{P}$, we have

$$\frac{\partial Z_k}{\partial D_{js}} = \frac{\partial Z_k}{\partial D_j} = -\frac{\partial Z_k}{\partial Y_j}$$

and

$$\frac{\partial \lambda}{\partial D_j} = -\frac{\partial \lambda}{\partial Y_j}.$$

Note that the FOC of final goods producers will satisfy

$$p_{js}q'_{js}(D_{js}) = p_j^{\mathcal{E},D}$$

and for unconstrained electricity generators we get

$$M'_j(Y_j^{\mathcal{E}}) = p_j^{\mathcal{E},S}.$$

So note that setting prices equal to

$$p_j^{\mathcal{E},D} = p_j^{\mathcal{E},S} = \sum_k \eta_k \frac{\partial Z_k}{\partial D_j} + \mu\left(1 + \frac{\partial \lambda}{\partial D_j}\right)$$

at unconstrained generating nodes will induce optimal behavior.

□

A5.3 Proof of Proposition 2

We proceed by showing that the market equilibrium with a number of utilities over connected sets of regions coincides with the solution to a global planner's problem under a certain set of Pareto weights. The problem of the global planner is

$$\max_{\{e^1_{js}, e^2_{js}, k_{js}, l_{js}, Y_j^{\mathcal{E}}, f_{js}, q_{j'js}\}} \quad \sum_j \Theta_j \prod_s \left(\sum_{j'} \left(\frac{q_{jj's}}{\tau_{jj's}}\right)^{\sigma-1} \right)^{\frac{\beta_{js}}{\sigma-1}}$$

for a fixed amount of total fossil fuel inputs $\bar{F}$, where Θ_j is the Pareto weight on region j, subject to the following constraints

$$\sum_{j'} q_{j'js} = z_{js} \left(e^1_{js}\right)^{v^{\mathcal{E}}_{js}} \left(\kappa_{js} \left(e^2_{js}\right)^{\frac{\psi-1}{\psi}} + f_{js}^{\frac{\psi-1}{\psi}}\right)^{\frac{\psi}{\psi-1} v^{\mathcal{F}}_{js}} k_{js}^{v^K_{js}} l_{js}^{v^L_{js}}$$

$$\sum_j \sum_s f_{js} + \sum_j G_j(K^{\mathcal{F}}_j, Y^{\mathcal{E}}_j - \theta K^{\mathcal{R}}_j) = \bar{F}$$

$$\sum_s l_{js} = L_{js}$$

$$\sum_s k_{js} = K_{js}$$

$$\sum_{j\in\mathcal{T}} \sum_s (e^1_{js} + e^2_{js}) + \boldsymbol{P'} \bar{\boldsymbol{B}}_{\mathcal{T}} \boldsymbol{P} = \sum_{j\in\mathcal{T}} Y^{\mathcal{E}}_j$$

$$-\boldsymbol{Z}^{max}_{\mathcal{T}} \leq \bar{\boldsymbol{\Omega}}_{\mathcal{T}} \bar{\boldsymbol{A}}_{\mathcal{T}} (\bar{\boldsymbol{A}}_{\boldsymbol{\mathcal{T}}}{}' \bar{\boldsymbol{\Omega}}_{\mathcal{T}} \bar{\boldsymbol{A}}_{\mathcal{T}})^{-1} \boldsymbol{P}_{\mathcal{T}} \leq \boldsymbol{Z}^{max}_{\mathcal{T}}$$

$$P_j = Y^{\mathcal{E}}_j - \sum (e^1_{js} + e^2_{js})$$

$$Y^{\mathcal{E}}_j \leq Y^{max}_j \tag{A11}$$

The first order conditions for the global planner for the amount of sectoral location goods $q_{j,j's}$ shipped from j' to j are

$$q_{jj's}: \quad \Theta_j \beta_{js} \prod_s \left(\sum_{j'} q^{\sigma-1}_{j,j's} \right)^{\frac{\beta_{js}}{\sigma-1}-1} \left(\frac{q_{j,j's}}{\tau_{jj's}}\right)^{\sigma-2} = \tau_{jj's} \mu^q_{j's} \tag{A12}$$

where $\mu^q_{j's}$ denotes the Lagrange multiplier on the resource constraint on sector s good from j'. Similarly, we can derive the first order condition for total sectoral electricity demand $D_{js} = e^1_{js} + e^2_{js}$ as

$$D_{js}: \quad \mu^q_{js} \frac{y_{js}}{D_{js}} \left(\kappa + (\frac{\kappa \mu^F}{\mu^E_{\mathcal{T}}})^{1-\psi}\right)^{\frac{\psi}{\psi-1} v^{\mathcal{F}}_{js}} (1 + \frac{v^E}{v_F})^{-v^{\mathcal{E}}_{js} + v^{\mathcal{F}}_{js}} = \mu^E_{\mathcal{T}} (1 + \frac{d\lambda_{\mathcal{T}}}{dD_{j,s}}) + \sum_{l\in\mathcal{T}} \frac{\partial Z_l}{\partial D_{j,s}} \mu^Z_l \tag{A13}$$

$$D_{js} = e^1_{j,s} (1 + \frac{v^{\mathcal{E}}_{js}}{v^{\mathcal{F}}_{js}})$$

where $\mu^E_{\mathcal{T}}$ is the Lagrange multiplier resource constraint on total electricity in network $\mathcal{T}$, and μ^F the Lagrange multiplier on the constraint for fossil fuels, and μ^Z_l the mulitplier on the constraint on capacity for line l. Meanwhile, the usage of fossil fuels within sector satisfy

$$\mu^E_{\mathcal{T}} \left(1 - \frac{d\lambda_{\mathcal{T}}}{dY_j}\right) = \mu^F \frac{\partial G_j}{\partial Y^{\mathcal{F}}} (K_j, Y^{\mathcal{E}}_j - \theta_j K^{\mathcal{R}}_j) + \mu^{max}_j \tag{A14}$$

where μ^F is the multiplier on the constraint on fossil fuel usage, and μ^{max}_j is the multiplier on the maximum power output in j.

The FOC's for labor and capital allocations across sectors within j are

$$\mu^q_{js} v^K_{js} \frac{y_{js}}{k_{js}} = \mu^K_j \quad \mu^q_{js} v^L_{js} \frac{y_{js}}{l_{js}} = \mu^L_j \tag{A15}$$

and the condition for fossil fuel usage is

$$\mu^q_{js} v^{\mathcal{F}}_{js} \frac{y_{js}}{\left(\kappa_{js,t} \left(e^2_{js}\right)^{\frac{\psi-1}{\psi}} + f_{js}^{\frac{\psi-1}{\psi}}\right) f_{js}^{\frac{-1}{\psi}}} = \mu^F \tag{A16}$$

Lastly, it to straightforward to show that the social planner maximizes a strictly concave objective function over a convex set, and as such the solution exists and is unique. Moreover, any vector $\{\{e^1_{js}, e^2_{js}, k_{js}, l_{js}, Y^{\mathcal{E}}_j, f_{js}, q_{j'js}\}, \{\mu^q_{js}, \mu^L_j, \mu^K_j, \mu^F, \mu^{max}_j\}\}$which satisfies both the FOCs above, the resource constraints and complementary slackness conditions is this solution. We now show an equivalence of these conditions with the equations governing the market equilibrium. First, the expenditure allocation problem of the consumer in j is

$$\max_{\{q^c_{j,j's}\}} \quad \prod_s \left((\sum_{j'} (q^c_{j,j's})^{\sigma-1})^{\frac{1}{\sigma-1}} \right)^{\beta_{js}}$$

subject to

$$\sum_{j'} \sum_s p_{j,j's} q^c_{j,j's} = E_j \tag{A17}$$

which has the FOC for $q^c_{j,j's}$ as

$$\beta_{js} \left(\sum_{j'} q^{\sigma-1}_{j,j's} \right)^{\frac{\beta_{js}}{\sigma-1}-1} (q^c_{j,j's})^{\sigma-2} = p_{j,j's} \Lambda_j, \tag{A18}$$

where $p_{j,j's}$ is the price of good $j's$ in location j and Λ_j is the Lagrange multiplier on the expenditure constraint of j in A17.

Second, the problem of the utility planner is

$$\max_{\{D_{js}, Y^F_j\}} \sum_j p_{js} q_j(D_{js}) - \sum_j p^{\mathcal{F}} G_j(Y^{\mathcal{E}}_j - \theta_j K^{\mathcal{R}}_j)$$

dsubject to

$$\sum_j Y^{\mathcal{E}}_j - \sum_j \sum_s D_{js} = \boldsymbol{P'} \bar{\boldsymbol{B}}_{\mathcal{T}} \boldsymbol{P}$$

$$-\boldsymbol{Z}^{max}_{\mathcal{T}} \leq \bar{\boldsymbol{\Omega}}_{\mathcal{T}} \bar{\boldsymbol{A}}_{\mathcal{T}} (\bar{\boldsymbol{A}}_{\boldsymbol{\mathcal{T}}}{}' \bar{\boldsymbol{\Omega}}_{\mathcal{T}} \bar{\boldsymbol{A}}_{\mathcal{T}})^{-1} \boldsymbol{P}_{\mathcal{T}} \leq \boldsymbol{Z}^{max}_{\mathcal{T}}$$

$$Y^{\mathcal{E}}_j \leq Y^{max}_j$$

The FOCs for this problem are

$$p_{js}q_j'(D_{js}) = \tilde{\mu}^{\mathcal{E}}_{\mathcal{T}}(1 + \frac{d\lambda_{\mathcal{T}}}{dD_{j,s}}) + \sum_{l\in\mathcal{T}} \frac{\partial Z_l}{\partial D_{j,s}}\tilde{\mu}^Z_l$$

$$p^{\mathcal{F}}\frac{\partial G_j}{\partial Y^{\mathcal{F}}}(K_j, Y^{\mathcal{E}}_j - \theta_j K^{\mathcal{R}}_j) = \tilde{\mu}^{\mathcal{E}}_{\mathcal{T}}(1 + \frac{d\lambda_{\mathcal{T}}}{dY^{\mathcal{E}}_j}) + \sum_{l\in\mathcal{T}} \frac{\partial Z_l}{\partial Y^{\mathcal{E}}_j}\tilde{\mu}^Z_l$$

Third, the first order conditions for the representative firm satisfy, in equilbrium,

$$p_{js}v^K_{js}\frac{y_{js}}{k_{js}} = \mu^K_j$$

$$p_{js}v^L_{js}\frac{y_{js}}{l_{js}} = \mu^L_j$$

and the condition for fossil fuel usage is

$$p_{js}v^{\mathcal{F}}_{js}\frac{y_{js}}{\left(\kappa_{js,t}\left(e^2_{js}\right)^{\frac{\psi-1}{\psi}} + f_{js}^{\frac{\psi-1}{\psi}}\right)f_{js}^{\frac{-1}{\psi}}} = p^{\mathcal{F}}$$

$$D_{js}: \quad p^q_{js}\frac{y_{js}}{D_{js}}\left(\kappa + (\frac{\kappa p^{\mathcal{F}}}{p^{\mathcal{E}}_j})^{1-\psi}\right)^{\frac{\psi}{\psi-1}v^{\mathcal{F}}}(1 + \frac{v^{\mathcal{E}}_{js}}{v^{\mathcal{F}}_{js}})^{-v^{\mathcal{E}}_{js}+v^{\mathcal{F}}_{js}} = p^{\mathcal{E}}_j$$

$$D_{js} = e^1_{j,s}(1 + \frac{v^{\mathcal{E}}_{js}}{v^{\mathcal{F}}_{js}})$$

Finally, there are three sets of market clearing conditions,

$$\sum_{j'} q_{j'js} = z_{js}\left(e^1_{js}\right)^{v^{\mathcal{E}}_{js}}\left(\kappa_{js}\left(e^2_{js}\right)^{\frac{\psi-1}{\psi}} + f_{js}^{\frac{\psi-1}{\psi}}\right)^{\frac{\psi}{\psi-1}v^{\mathcal{F}}_{is}} k_{js}^{v^K_{js}} l_{js}^{v^L_{js}}$$

$$\sum_s l_{js} = L_{js}$$

$$\sum_s k_{js} = K_{js}$$

Now we show an equivalence between these two sets of conditions. Suppose that the Pareto weight on j is equal to the inverse marginal utility of wealth in j in the competitive allocation Λ_j^{-1}. Since it is straightforward to show that the planner maximize a strictly concave function over a strictly convex set, there is a single solution that solves the planning problem.

Then via relabelling, the same equations can be seen to describe the planners allocation (A13) and the competitive allocation for goods must yield the same values for the Lagrange multiplier when evaluated at the competitive equilibrium quantities.